ENDOTHELIAL PROX1 INDUCES BLOOD-BRAIN BARRIER DISRUPTION IN THE CENTRAL NERVOUS SYSTEM

Sara González-Hernández[1], Ryo Sato[1], Yuya Sato[1, 5], Chang Liu[1, 6], Wenling Li[1], Chengyu Liu[2], Sadhana Jackson[3], Yoshiaki Kubota[4], Yoh-suke Mukouyama[1*]

[1]Laboratory of Stem Cell and Neuro-Vascular Biology, Cell and Developmental Biology Center, National Heart, Lung, and Blood Institute, National Institutes of Health, Bethesda, MD, USA

[2]Transgenic Core, National Heart, Lung, and Blood Institute, National Institutes of Health, Bethesda, MD, USA

[3]Developmental Therapeutics and Pharmacology Unit, Surgical Neurology Branch, National Institute of Neurological Disorders and Stroke, National Institutes of Health, Bethesda, MD, USA

[4]Department of Anatomy, Institute for Advanced Medical, Research and Keio University School of Medicine, Shinjuku, Tokyo, Japan

[5]Present Address: Knowledge Palette, Inc. Kobe, Hyogo, Japan

[6]Present Address: Sarepta Therapeutics, Inc. Durham, NC, USA

[*]Author for correspondence:

Yoh-suke Mukouyama

E-mail: mukoyamay@mail.nih.gov

Tel: +1 301 451 1663

Conflict-of-interest statement:

The authors have declare that no conflict of interest exists.

ABSTRACT

The central nervous system (CNS) parenchyma has conventionally been believed to lack lymphatic vasculature, likely due to a non-permissive microenvironment that hinders the formation and growth of lymphatic endothelial cells (LECs). Recent findings of ectopic expression of LEC markers including Prospero Homeobox 1 (PROX1), a master regulator of lymphatic differentiation, and the vascular permeability marker Plasmalemma Vesicle Associated Protein (PLVAP), in certain glioblastoma and brain arteriovenous malformations (AVMs), has prompted investigation into their roles in cerebrovascular malformations, tumor environments, and blood-brain barrier (BBB) abnormalities. To explore the relationship between ectopic LEC properties and BBB disruption, we utilized endothelial cell-specific *Prox1* overexpression mutants. When induced during embryonic stages of BBB formation, endothelial *Prox1* expression induces hybrid blood-lymphatic phenotypes in the developing CNS vasculature. This effect is not observed when *Prox1* is overexpressed during postnatal BBB maturation. Ectopic *Prox1* expression leads to significant vascular malformations and enhanced vascular leakage, resulting in BBB disruption when induced during both embryonic and postnatal stages. Mechanistically, PROX1 downregulates critical BBB-associated genes, including *ß-catenin* and *Claudin-5*, which are essential for BBB development and maintenance. These findings suggest that PROX1 compromises BBB integrity by negatively regulating BBB-associated gene expression and Wnt/ß-catenin signaling.

INTRODUCTION

The central nervous system (CNS), comprising both the brain and spinal cord, develops a specialized vascular network characterized by the presence of specialized endothelial cells (ECs) that constitute the blood-brain barrier (BBB) and the absence of lymphatic vasculature within the parenchyma. This barrier serves as a formidable separation blockade, dividing the CNS from the peripheral blood circulation (reviewed in(1-5)). The ECs comprising the BBB exhibit distinctive features compared to ECs in the other tissues: they possess continuous intercellular tight junction (TJ) proteins, lack fenestrations, and display minimal transcytosis activity(1-5). Furthermore, it is plausible that the absence of classical, highly permeable lymphatic capillaries, which are composed of lymphatic ECs (LECs) with discontinuous button-like junctions, impedes the induction of an immune response to CNS-derived antigens. This establishes the CNS parenchyma as an organ with immune-privileged status(6-8). Blood and lymphatic vasculature are closely associated in non-CNS tissues; however, the link between BBB integrity and lymphatic avascularity in the CNS parenchyma remains poorly understood.

LEC specification relies on the action of the homeobox transcription factor PROX1, which is necessary and sufficient to induce the LEC development program and repress the blood EC (BEC) development program in vitro and in vivo(9-15). Notably, LEC identity can be reprogrammed back into BEC identity by downregulating the expression of PROX1 during embryonic, postnatal, or adult stages(13). While the CNS parenchyma is considered an organ devoid of lymphatic vasculature, recent studies demonstrate that PROX1^{+} lymphatic vasculature develops an extensive network in the dura mater of

meninges under the skull(16-19), and PROX1^{+} non-lumenized mural LECs, also called brain LECs or fluorescent granule perithelial cells, develop in the surface of zebrafish brain and mammalian leptomeninges(20-24). In several pathological conditions, including glioblastoma and brain arteriovenous malformations (AVMs), LEC markers including PROX1 are upregulated in ECs (25-27). Given that BBB integrity is often compromised in these glioblastoma and AVMs, these findings suggest a potential link between ectopic LEC marker expression and BBB disruption. Under normal physiological conditions, suppression of LEC properties may be essential for the development and maintenance of BBB in the CNS parenchyma. However, in pathological conditions, the ectopic upregulation of LEC markers might contribute to BBB disruption, thereby promoting disease progression.

In this study, we first analyzed publicly available single-cell RNA sequencing (scRNA-seq) data from human samples exhibiting impaired BBB integrity, including cases of AVMs, brain metastases, and glioblastoma tumors. Our analysis reveals upregulation lymphatic markers (*PROX1*, *LYVE1, FLT4*) in the CNS vasculature across these diseases associated with BBB dysfunction, alongside increased levels of *Plasmalemma Vesicle Associated Protein* (*PLVAP*), a factor commonly linked to endothelial permeability and BBB disruption. To explore the link between ectopic LEC differentiation in the CNS parenchyma and BBB disruption, we utilized a mouse model to express *Prox1* transgene, the master regulator of LEC development, in CNS ECs during BBB formation or maintenance. EC-specific overexpression of *Prox1* in mice results in significant alterations in the morphology and barrier function of the CNS vasculature.

Interestingly, endothelial *Prox1* expression induces a hybrid blood-lymphatic phenotype, characterized by the expression of both BEC markers and a subset of LEC markers, in the developing CNS vasculature when induced during primitive BBB formation at embryonic stages. However, such a hybrid blood-lymphatic phenotype is not observed when the *Prox1* expression is induced during the BBB maturation at postnatal stages. However, endothelial *Prox1* expression promotes enhanced vascular leakage and BBB disruption when induced during both embryonic and postnatal stages. This vascular leakage is attributed to the downregulation of TJ proteins and the upregulation of transcytosis, underscoring the inhibitory effects of PROX1 on the BBB development and maintenance. Our in vitro experiments using brain ECs provide mechanistic insights into how PROX1 influences EC barrier functions: *Prox1* overexpression leads to a significant reduction in the expression of the TJ protein Claudin-5 and a destabilization of the actomyosin cytoskeleton, resulting in aberrant cell-cell junction formation. At the molecular level, PROX1 reduces the mRNA expression of BBB-associated genes, including *ß-catenin*, which is a critical signaling component for BBB development and maintenance. PROX1 disrupts BBB integrity through negative regulation of BBB-associated gene expression and Wnt/ß-catenin signaling. Collectively, our studies highlight the potential clinical impact of *Prox1* regulation in the CNS vasculature.

RESULTS

Lymphatic endothelial cell markers are upregulated in endothelial cells within brain tumors and vascular malformations.

We analyzed publicly available single-cell RNA-seq (scRNA-seq) datasets from human glioblastoma (28-30), tumor metastases (31) and AVMs (32) to assess the expression of lymphatic endothelial cell (LEC) markers in endothelial cells (ECs) (Figure 1A and Supplemental Figure 1). After extracting ECs from three glioblastoma datasets and integrating them, we observed *PROX1* expression in ECs within the tumors, accompanying other lymphatic marker expressions (*LYVE1* and *FLT4*) (Figure 1B; Supplemental Figure 1, A-B). The tumor metastasis and AVM datasets each comprised disease (red) and control (blue) conditions, enabling comparisons between these states (Figure 1, C-D and Supplemental Figure 1, C-F). Examination of lymphatic marker genes revealed a pronounced increase in *PROX1* expression under disease conditions in both datasets. Additionally, we observed increased levels of *PLVAP*, which is commonly associated with endothelial permeability and BBB disruption(33-35), in ECs over all three disease conditions (Figure 1, B-D; Supplemental Figure 1, A-F). Also, downregulation of the BBB-associated markers (*CTNNB1* and *CLDN5*) was observed in disease conditions compared to control ECs (Supplemental Figure 1, D and F). These data suggest that abnormal differentiation from blood vessels to lymphatic vessels in the CNS may be connected to vascular permeability and BBB disruption observed in these conditions.

Mouse CNS parenchyma lacks lymphatic vessels and does not exhibit temporal expression of PROX1 in its vasculature under physiological conditions.

To investigate a potential link between ectopic LEC differentiation in the CNS parenchyma and BBB disruption, we turned to a mouse model to manipulate *Prox1*

expression in the brain vasculature during primitive BBB formation at embryonic stages, or BBB maturation at postnatal stages. Given that the aforementioned scRNA-seq analysis from normal human brain samples revealed *PROX1* expression in a subset of brain ECs, we first examined PROX1 expression in the parenchymal vasculature of the mouse brain and spinal cord during embryonic or postnatal stages.

We performed high-resolution whole-mount imaging of mouse embryonic brains using the *Prox1-Gfp BAC* transgenic reporter(36), which allows visualization of PROX1-expressing cells with the green fluorescent protein (GFP). Since PROX1 is also expressed in neural progenitors and is recognized for its involvement in neuronal differentiation in the CNS(37), we defined PROX1-expressing ECs as those showing co-localization of GFP expression with both the pan-EC marker PECAM1 and the nuclear EC marker ERG. We also performed immunostaining using anti-PROX1 antibody to validate that the GFP signal corresponded to PROX1 expression. Section immunostaining of the *Prox1-Gfp* brain and spinal cord at embryonic stage (E)13.5 reveals that ERG^+ EC-nuclei do not co-localize with PROX1 and Prox1-GFP, whereas there are numerous neural progenitors that are ERG-negative but positive for PROX1 and Prox1-GFP (Figure 2, A-C"; arrows indicate ERG^+ EC-nuclei). Likewise, in the spinal cord parenchyma, ERG^+ EC-nuclei do not co-localize with PROX1 and Prox1-GFP (Figure 2, D-E', arrows). At E15.5, we did not observe any apparent co-localization of Prox1-GFP and the EC markers PECAM1 and ERG within a cluster of Prox1-GFP^+ neural progenitors in the brain parenchyma (Figure 2F; arrows indicate ERG^+/$PECAM1^+$ ECs). The absence of PROX1 expression within the brain vasculature was confirmed

during postnatal stages (Figure 2G). Of note, the combination of PECAM1 and LYVE1 allows us to corroborate the absence of classical lymphatic vessels (PECAM1^{+}/LYVE1^{+}/Prox1-GFP^{+}) inside the brain parenchyma at postnatal stage (P)3, where only PECAM1^{-}/LYVE1^{+}/Prox1-GFP^{-} macrophages were found in the perivascular space (Figure 2, G-H, yellow arrowheads; Supplemental Figure 2, A-C). In contrast, PECAM1^{+}/LYVE1^{+}/Prox1-GFP^{+} lymphatic vessels were observed in both the meningeal layers and head skin vasculature (Figure 2, I-J, arrowheads; Supplemental Figure 2, D-H, arrows). Combined, this time-course analysis not only reaffirms the dearth of lymphatic vasculature within the CNS parenchyma but also underscores the absence of the lymphatic master regulator PROX1 in the CNS parenchyma ECs.

Endothelial *Prox1* expression leads to severe vascular abnormalities in the developing CNS vasculature.

To address the relationship between PROX1 expression and BBB development/maintenance in a non-disease context, we generated a conditional *Prox1* overexpression mouse harboring the *loxP-STOP-loxP-Prox1* cassette in the *Rosa26* locus (*R26-LSL-Prox1* mice)(38), that allowed us to induce *Prox1* expression in a time- and cell type-specific manner (Supplemental Figure 3A). We further crossed them with the EC-specific *Cdh5-BAC-Cre^{ERT2}* driver mice(39) to induce the *Prox1* transgene in ECs. Because previous studies have shown that primitive BBB becomes functional in the developing brain vasculature around E15.5(40), we opted to induce the *Prox1* transgene in *R26-LSL-Prox1* embryos (hereafter referred to as *Prox1$^{iEC\text{-}OE}$*) through a

tamoxifen administration at E13.5 and examine the resulting impact on brain vasculature development and BBB integrity at E16.5 (Figure 3A).

The resulting *Prox1*$^{iEC\text{-}OE}$ mutant embryos exhibited pronounced edemas, hemorrhagic manifestation, and blood-filled lymphatics in the skin (Figure 3A; Supplemental Figure 3B). Moreover, the mutants exhibited embryonic lethality within 72 hours following the *Prox1* transgene induction in ECs (Supplemental Figure 3B). We validated the efficient induction of the *Prox1* transgene in PECAM1^{+} ECs of the brain vasculature in *Prox1*$^{iEC\text{-}OE}$ mutant embryos, whereas *Prox1* expression was absent in PECAM1^{+} ECs in their *wild-type* (WT) control littermates (Figure 3B). A sagittal overview reveals significant disparities in the brain vasculature between *Prox1*$^{iEC\text{-}OE}$ mutant embryos and their WT control littermates, notably in the cerebral cortex region where abnormal enlarged vessels are present, while capillary density is reduced in the mutants (Figure 3, C-G, yellow arrowheads; Supplemental Figure 3, C-H). Immunostaining with antibodies to the adherent junction marker ZO-1 and the nuclear EC marker ERG reveals the formation of thick capillaries due to an augmented number of ECs in *Prox1*$^{iEC\text{-}OE}$ mutant embryos, as compared to their WT control littermates (Figure 3, H-I).

We next investigated whether *Prox1* expression induces a LEC fate in the vasculature of *Prox1*$^{iEC\text{-}OE}$ mutant embryos. We first examined the expression of the classical LEC marker LYVE1 in the vasculature of *Prox1*$^{iEC\text{-}OE}$ mutant embryos and their WT control littermates. We observed a substantial increase in PECAM1^{+}/LYVE1^{+} lymphatic vessels in the trunk vasculature of the mutant embryos compared to their WT control littermates

(Figure 4A, arrows). In contrast, we did not detect any LYVE1-expressing ECs in the brain vasculature of either the mutant embryos or their WT control littermates (Figure 4B). Quantitative validation of these findings was achieved through flow cytometry analysis (Supplemental Figure 4, A-B): PECAM1^{+}/LYVE1^{+} LECs were not detectable in both the mutant and control brain (comprising 0% of brain ECs), whereas the mutant skin exhibited a significant increase in the proportion of LYVE1^{+}/PECAM1^{+} LECs (from 5% to 30% of skin ECs) alongside a concurrent decrease in LYVE1^{-}/PECAM1^{+} BECs (from 95% to 70% of skin ECs). These data suggest that consistent with the established propensity of PROX1 function to evoke lymphatic differentiation in the developing vasculature, endothelial *Prox1* expression induces the differentiation of BECs into LECs in the skin vasculature. In contrast, in the brain vasculature, *Prox1* does not induce conventional LECs. While *Prox1* induces significant remodeling in the brain parenchymal vasculature, characterized by the rapid development of enlarged vessels and thicker capillaries, particularly in the cerebral cortex region, it appears that *Prox1* expression alone is insufficient to induce conventional LECs expressing the classical LEC markers such as LYVE1 (Figure 4B) and podoplanin (PDPL, data not shown).

Of note, given our use of the EC-specific *Cdh5-BAC-Cre^{ERT2}* driver mice to induce the *Prox1* transgene in ECs, we observed abnormalities in the lymphatic vasculature in peripheral tissues. For instance, whole-mount immunostaining of limb skin and heart ventricles revealed aberrant branching of lymphatic vessels in *Prox1$^{iEC\text{-}OE}$* mutant embryos (Supplemental Figure 4, C-E). As previously described(41), LYVE1^{+}/PECAM1^{+} cardiac lymphatic vessels extend inferior on both the ventral and dorsal surfaces of the

heart ventricle in the WT control littermates (Supplemental Figure 4D, arrows). Notably, some of these lymphatic vessels branch closely to EMCN$^+$/PECAM1$^+$ large-diameter coronary veins on the dorsal surface of the heart ventricle. In contrast, the ventral surface of the mutant heart ventricle exhibited blood-filled lymphatic vasculature, while the dorsal surface showed abnormal lymphatic structures (Supplemental Figure 4E). Additionally, the mutants exhibited underdeveloped coronary vasculature, characterized by the absence of large-diameter coronary arteries (Supplemental Figure 4, D-E, PECAM1$^+$, arrowheads) and veins (Supplemental Figure 4, D-E, EMCN$^+$, yellow arrowheads). These findings suggest that endothelial *Prox1* expression leads to abnormal coronary and cardiac lymphatic vasculature in the developing heart ventricles.

Endothelial *Prox1* expression induces a hybrid blood-lymphatic phenotype in the developing CNS vasculature.

In light of the recent discovery of Schlemm's canal in the eye, which is a specialized ring-shaped vasculature at the periphery of the cornea and has ECs having BEC and LEC characteristics, including the expression of BEC markers and a subset of LEC makers(42-44), we proceeded to examine whether *Prox1* expression induces a hybrid blood-lymphatic phenotype in the brain vasculature. Schlemm's canal ECs manifest the expression of BEC markers including PECAM1, endomucin (EMCN), CD34, VE-Cadherin (Cdh5), and Tie2, and the expression of LEC markers such as PROX1, VEGFR3, and ITGα9. The classical LEC markers LYVE1 and PDPL are absent in Schlemm's canal ECs (Figure 4C). Additionally, plasmalemma vesicle-associated

protein (PLVAP), a component of endothelial fenestrae that regulates basal permeability(33-35), is highly expressed Schlemm's canal ECs (Figure 4C).

In the brain vasculature of WT control littermates, the expression of PLVAP, VEGFR3, and ITGα9 is scarcely detectable in ECs (Figure 4, D-E; overlap with the pan-EC markers ERG and PECAM1, or the pan-capillary EC marker EMCN). In contrast, in the brain vasculature of *Prox1*$^{iEC\text{-}OE}$ mutant embryos, the expression of these markers is substantially upregulated compared to their WT control littermates (Figure 4D; quantification in Figure 4E). At the mRNA level, brain ECs isolated through fluorescence-activated cell sorting (FACS) from *Prox1*$^{iEC\text{-}OE}$ mutant embryos demonstrate increased expression of *Plvap* compared to their WT control littermates (Figure 4F). Although the expression of BEC markers such as *VE-Cadherin*/*Cdh5*, *Cd34*, *Itgα5,* and *Gata2* is partially reduced in FACS-isolated brain ECs from *Prox1*$^{iEC\text{-}OE}$ mutant embryos compared to their WT control littermates (Figure 4F), it is evident that endothelial *Prox1* expression does not completely reprogram BECs to LECs in the brain vasculature. Taken together, this evidence shows that *Prox1* induces a hybrid blood-lymphatic phenotype in the brain vasculature, reminiscent of Schlemm's canal ECs in the eyes, with the expression of BEC (PECAM1^{+}/PLVAP^{+}) and LEC (PROX1^{+}/VEGFR3^{+}/ITGα9^{+}) markers.

Endothelial expression of *Prox1* disrupts primitive blood-brain barrier formation in the developing CNS vasculature.

CNS ECs express the tight junction (TJ) protein Claudin-5 (CLDN5) as a marker for BBB, while PLVAP, inductive of high-permeability vasculature, is normally absent from these cells(5, 45). In regions of the brain where the BBB is compromised, there is a reduction in CLDN5 expression and an induction of PLVAP(5, 46). We then investigated whether the acquisition of such a hybrid blood-lymphatic phenotype in the CNS vasculature of *Prox1*$^{iEC\text{-}OE}$ mutant embryos might affect the development and integrity of the BBB.

Immunostaining with antibodies to the TJ marker CLDN5 and the pan-EC marker ERG clearly demonstrates a reduction in CLDN5 expression in the brain vasculature of *Prox1*$^{iEC\text{-}OE}$ mutant embryos as compared to their WT control littermates (Figure 5A; quantification in Figure 5B). This reduction indicates impaired TJ assembly among cerebral ECs, suggesting a defect in barrier integrity. Moreover, Ter119^{+} blood cell extravasation was observed in *Prox1*$^{iEC\text{-}OE}$ mutant brains (Supplemental Figure 5, A-C, arrows). These data indicate a potential compromise in the BBB. To further address whether the mutant brains exhibited compromised barrier function, we performed a tracer leakage assay in E16.5 *Prox1*$^{iEC\text{-}OE}$ mutant embryos and their WT control littermates when the primitive BBB becomes functional(40). We harvested embryos and performed an intracardial injection of a 3kDa fluorescent tracer, Dextran Texas-Red (Figure 5C). Whole brain images and subsequent immunostaining of sagittal brain samples reveal extensive BBB leakage in *Prox1*$^{iEC\text{-}OE}$ mutant embryos (Figure 5, D-H; quantification in Figure 5I; Supplemental Figure 5, D-F): The injected dextran tracer remained entirely within PECAM1^{+} vasculature of WT control littermates (Figure 5, D-F

and Supplemental Video 1), while severe BBB leakage was observed in the mutant embryos, particularly within the cerebral cortex (Figure 5, D-H and Supplemental Video 2). These findings suggest that the endothelial *Prox1* expression disrupts primitive BBB formation in the developing CNS vasculature.

We next assessed the mRNA expression of BBB markers in FACS-isolated ECs from *Prox1*$^{iEC\text{-}OE}$ mutant brains and their WT control littermates. We observed a decrease in the expression of TJ markers *Cldn5* and *Tjp1/ZO-1* in *Prox1*$^{iEC\text{-}OE}$ mutant embryos compared to their WT control littermates (Figure 5J). We also observed a decrease in the expression of recently identified BBB-related genes, such as *Cd93(47)* and *Fgfpd1(48)* in the mutant embryos compared to their WT control littermates (Figure 5J). Additionally, we found a reduction in the expression of the lipid transporter *Mfsd2a*, which plays an essential role in limiting caveolin-dependent transcytosis in BBB ECs(40, 49-51) in the mutant embryos compared to their WT control littermates. Furthermore, the expression of *Pten*, which serves as an upstream regulator of the Mfsd2a-transcytosis axis(51), was also downregulated in the mutant embryos (Supplemental Figure 5G). This finding suggests a potential upregulation of transcytosis in addition to an impaired TJ in the mutant embryos (Figure 5J). Given that Wnt/ß-catenin signaling is known to regulate many BBB genes including *Cldn5*, *Plvap*, and *Mfsd2a*(1, 4, 5), we observed a decrease in the expression of *Ctnnb1/ß-catenin* as well as several effector and target genes associated with Wnt/ß-catenin signaling in the mutant embryos compared to their WT control littermates (Figure 5K and Supplemental Figure 5G).

These results indicate that the endothelial *Prox1* expression leads to a significant downregulation of Wnt/ß-catenin signaling in the developing CNS vasculature.

Pericyte-EC association is essential for the formation of a functionally effective BBB(52, 53). Thus, barrier defects in *Prox1*$^{iEC\text{-}OE}$ mutant embryos could be due to altered pericyte coverage of capillaries. However, immunostaining with antibodies to the pericyte markers NG2 and PDGFRß, in combination with PECAM1, reveals pericyte coverage of enlarged capillaries in the brain vasculature of *Prox1*$^{iEC\text{-}OE}$ mutant embryos (Supplemental Figure 5, H-K, arrows). Indeed, FACS analysis reveals a comparable number of CD140b(PDGFRß)$^{+}$/CD31(PECAM1)$^{-}$ pericytes in both *Prox1*$^{iEC\text{-}OE}$ mutant embryos and their WT control littermates, exhibiting a similar maximal fluorescence intensity (MFI) corresponding to the expression of the pericyte marker CD140b (Supplemental Figure 5, L-M). Of note, immunostaining with the anti-NG2 antibody also labels oligodendrocytes (NG2^{+}/PDGFRß$^{-}$) (Supplemental Figure 5, H-K, yellow arrowheads), and we observed an increased association between oligodendrocytes and capillaries (Supplemental Figure 5, I and K, yellow arrowheads) in *Prox1*$^{iEC\text{-}OE}$ mutant embryos compared to their WT control littermates. Given that previous studies have reported the expression of Wnt7a/b ligands for canonical Wnt/ß-catenin signaling(54-56) by oligodendrocytes, in addition to astroglia and neurons, these findings suggest that oligodendrocytes may play a role in repairing BBB disruption.

Postnatal induction of *Prox1* leads to blood-brain barrier breakdown.

The observation that the endothelial *Prox1* expression during primitive BBB formation leads to the BBB disruption prompted us to investigate whether PROX1 itself exerts any influence on BBB function after it has already formed and matured, even in the absence of LEC differentiation in the CNS parenchyma. To address this question, we opted to induce the *Prox1* transgene through tamoxifen administration during BBB maturation at postnatal stage (P)7 and examine the resulting impact on BBB integrity. We performed a tracer leakage assay in P10 *Prox1*$^{iEC\text{-}OE}$ mutant mice and their WT control littermates: We performed an intraperitoneal injection (I.P.) of a 3kDa Dextran Texas-Red or a 1kDa Alexa Fluor 555-Cadaverine (Figure 6A). Brightfield whole brain images show enlarged vessels in *Prox1*$^{iEC\text{-}OE}$ mutant brains (Figure 6B). Whole-mount immunostaining and tissue clearing of sagittal brain samples with antibodies to the EC markers PECAM1 or EMCN reveals extensive BBB leakage in *Prox1*$^{iEC\text{-}OE}$ mutant brains (Figure 6, D-F; quantification in Figure 6C). Severe BBB leakage was observed within the cerebellum of the mutant mice (Figure 6, E-E' and F-F'). Subsequent section immunostaining of the cerebellum clearly demonstrates that the dextran tracer leaks out of vessels in the mutant mice (Figure 6G). We also observed similar leakage in the 1kDa Alexa Fluor 555-cadaverine tracer (Supplemental Figure 6B; quantification in Supplemental Figure 6D). These results show that the endothelial *Prox1* expression disrupts barrier function in the postnatal CNS vasculature.

We next investigated whether the *Prox1* expression impacts capillary network and BBB integrity. While the brain of the WT control littermate featured a dense capillary network, the mutant brain exhibited abnormally enlarged vasculature with reduced vascular

density and larger caliber vessels (Supplemental Figure 6A). However, we did not detect any significant change in the mRNA expression of BEC markers such as *VE-Cadherin*/*Cdh5*, *Cd34*, *Itgα5,* and *Gata2* between *Prox1*$^{iEC\text{-}OE}$ mutants and their WT control littermates (Supplemental Figure 6F). Moreover, we also did not observe a hybrid blood-lymphatic phenotype in the postnatal brain vasculature of *Prox1*$^{iEC\text{-}OE}$ mutants: we did not find upregulation of LEC markers such as VEGFR3 and ITGα9, as was observed in the developing brain vasculature (Supplemental Figure 6, G-H). These findings suggest that the *Prox1* does not induce a hybrid blood-lymphatic phenotype in the postnatal brain vasculature.

Since impaired barrier function correlates with impaired TJ proteins, we observed a reduction in the expression of CLDN5 in the brain vasculature of *Prox1*$^{iEC\text{-}OE}$ mutants as compared to their WT control littermates (Supplemental Figure 6B; quantification in Supplemental Figure 6C). Supporting this observation, we also found a decrease in the mRNA expression of BBB markers, such as *Cldn5*, *Tjp1/ZO-1*, *Cd93*, *Fgfbp1,* and *Mfsd2a,* and an increase in the expression of *Plvap* and *Caveolin-1/Cav1,* in *Prox1*$^{iEC\text{-}OE}$ mutants compared to their WT control littermates (Figure 6H). These findings demonstrate that the endothelial *Prox1* expression disrupts barrier integrity in the postnatal CNS vasculature.

Given that EC ß-catenin signaling is known to maintain the BBB state(46, 57-60), we observed a decrease in the mRNA expression of *Ctnnb1/ß-catenin,* as well as several effector and target genes associated with Wnt/ß-catenin signaling in the mutants

compared to their WT control littermates (Figure 6I and Supplemental Figure 6E). Taken together with the findings from the analysis of the developing CNS vasculature, these data show that the endothelial *Prox1* expression significantly downregulates Wnt/ß-catenin signaling in both developing and postnatal CNS vasculature.

Recent observations indicating that Wnt/ß-catenin signaling activates *Mfsd2a* to limit caveolae-mediated transcytosis in CNS ECs(50, 51, 57, 61) prompted us to investigate whether the *Prox1* expression affects both transcellular and the aforesaid paracellular permeability in the postnatal CNS vasculature. Through transmission electron microscopy (TEM) analysis, we first observed an enlarged capillary lumen in *Prox1*$^{iEC\text{-}OE}$ mutants compared to their WT control littermates (Figure 6, J and K). Secondly, we verified an increased gap in TJ and an increased number of transcellular vesicles in ECs of the mutants in comparison to their WT control littermates (Figure 6K, yellow arrows). These data indicate that the endothelial *Prox1* expression induces BBB breakdown by enhancing both paracellular and transcellular permeability in the postnatal CNS vasculature.

Endothelial *Prox1* expression induces abnormal tight junctions by repressing *Claudin-5* expression and destabilizing actin filaments in brain endothelial cells.

We next explored how PROX1 disrupts EC barrier functions. To address this question, we turned to in vitro culture experiments using a mouse brain EC line, bEnd.3 cells, known for its brain EC-specific characteristics, including the maintenance of neural stem cells(62). Importantly, previous studies demonstrated that Wnt/ß-catenin signaling

upregulates the expression of *Mfsd2a*, while downregulating the expression of *Cav1* and *Plvap* in cultured bEnd.3 cells(57). Given that endogenous PROX1 expression was not detectable in bEnd.3 cells, we introduced the *Prox1* or *Gfp* transgene into the cells using a lentiviral system and subsequently cultured these infected cells until they formed confluent monolayers (Supplemental Figure 7, A-B). Most of the bEnd.3 cells expressing *Prox1* exhibited discontinuous cell-cell junctions and an enlarged cell shape, as determined with ZO-1 immunostaining, whereas the bEnd.3 cells expressing *Gfp* showed continuous yet reticular cell-cell junctions without altered cell shape (Figure 7, A-B; three representative images for each bEnd.3 cells expressing *Prox1* or *Gfp*). Since EC junctions are tightly regulated by actin cytoskeleton(63), we observed a significant reduction in the intensity of F-Actin (Figure 7, A-B and C-D) and phospho-myosin light chain 2 (p-MLC2), a downstream target of the RhoA/ROCK pathway that regulates actin stress fiber contraction and cytoskeleton remodeling, in the bEnd.3 cells expressing *Prox1* (Figure 7, C-D). These observations suggest that the *Prox1* expression leads to abnormal organization and a relaxation of actin stress fibers, resulting in the formation of enlarged cell shape and abnormal cell-cell junctions. Indeed, the bEnd.3 cells expressing *Prox1* not only exhibited discontinuous cell-cell junctions but also a marked reduction in CLDN5 expression. In contrast, the bEnd.3 cells expressing *Gfp* showed colocalization of ZO-1 and CLDN5 in continuous cell-cell junctions (Figure 7, E-F; quantification in Figure 7G). Of note, we also observed abnormal cell-cell junctions in most primary rat brain microvascular ECs expressing *Prox1* (RBMVECs) (Supplemental Figure 7, C-D). Collectively, these in vitro studies present compelling evidence of abnormal TJs because of the endothelial *Prox1* expression in brain ECs. Interestingly,

Prox1 also influences the actin cytoskeleton, promoting disorganized and relaxed actin fibers, which in turn result in less polarized and enlarged ECs. These observations may correspond to the formation of enlarged vessels and thicker capillaries in the CNS vasculature of *Prox1*$^{iEC\text{-}OE}$ mutant mice.

The foregoing in vivo and in vitro studies demonstrate that *Prox1* expression in brain ECs leads to a decrease in the mRNA expression of *Cldn5* and a reduction of both junctional and cytoplasmic CLDN5 in brain ECs (Figure 7, E-F, Supplemental Figure 8A). Considering prior reports that suggest PROX1 functions as a transcriptional repressor in neural progenitors(64), hepatocytes(65), and cancers(66, 67), it is plausible that PROX1 regulates CLDN5 expression through direct transcriptional suppression of *Cldn5* gene. Analysis of a published whole-genome chromatin immunoprecipitation sequencing (ChIP-seq) using an anti-PROX1 antibody in human umbilical vein ECs (HUVECs) expressing *Prox1* reveals the presence of PROX1-binding sites at the promoter of *Cldn5* gene(68) (Supplemental Figure 8A). Likewise, we demonstrate that the endothelial *Prox1* expression leads to a decrease in the mRNA expression of *Ctnnb1/ß-catenin* and *Cd93,* and the whole-genome Prox1 ChIP-seq reveals the presence of PROX1-binding site at the *Ctnnb1/ß-catenin* and *Cd93* promoters. These findings imply that PROX1 may inhibit the promoter of *Cldn5*, *Ctnnb1*, or *Cd93* gene in brain ECs. Conversely, although the mRNA expression of *Mfsd2a* is also downregulated in brain ECs of *Prox1*$^{iEC\text{-}OE}$ mutant mice, a PROX1-binding site was not identified in its promoter region (Supplemental Figure 8A). Considering that the expression of *Mfsd2a* is known to be transcriptionally regulated by Wnt/ß-catenin signaling, the decreased

454 expression of *Mfsd2a* in the mutants might be attributed to reduced ß-catenin level.
455 Taken together, these data suggest that *Prox1* expression in brain ECs disrupts barrier
456 integrity by reducing the expression of BBB-associated genes and Wnt/ß-catenin
457 signaling in brain ECs (Supplemental Figure 8B).
458
459 **DISCUSSION**
460 The immune privilege environment of the CNS parenchyma is maintained by unique
461 immunological barriers, including the presence of the BBB and the absence of lymphatic
462 vasculature. However, under pathological conditions such as brain tumors and AVMs,
463 which compromise vascular integrity, there is an upregulation of LEC markers, including
464 the LEC master regulator PROX1 and the vascular permeability marker PLVAP. Several
465 lines of evidence suggest that PROX1 impairs BBB integrity by negatively regulating the
466 expression of BBB-associated genes and Wnt/ß-catenin signaling. First, endothelial
467 *Prox1* expression induces a hybrid blood-lymphatic phenotype in the developing CNS
468 vasculature when activated during primitive BBB formation at embryonic stages,
469 whereas it does not induce this phenotype during the BBB maturation at postnatal
470 stages. Second, while *Prox1* is insufficient to induce conventional lymphatic vascular
471 formation within the CNS parenchyma, it disrupts BBB integrity by downregulating TJ
472 proteins and increasing transcytosis. These findings highlight the inhibitory effects of
473 PROX1 on BBB development and maintenance. Third, PROX1 negatively regulates the
474 expression of BBB-associated genes and Wnt/ß-catenin signaling in ECs.
475

Embryonic *Prox1* induction triggers the transformation of blood vessels into hybrid blood-lymphatic vessels, rather than the formation of conventional lymphatic vessels, within the brain parenchyma. Like Schlemm's canal ECs in the eyes, *Prox1*$^{iEC\text{-}OE}$ mutant ECs express the LEC markers such as VEGFR3 and ITGα9, but not LYVE1 or PDPN, as well as the BEC markers such as PECAM1, ERG, and EMCN. Interestingly, the induction of *Prox1* postnatally does not result in a hybrid blood-lymphatic phenotype within the brain parenchyma, as *Prox1*$^{iEC\text{-}OE}$ mutant ECs fail to upregulate the expression of VEGFR3 and ITGα9. Given that the VEGF-C/VEGFR3 signaling is crucial for the early development of Schlemm's canal ECs(42, 43), the lower VEGFR3 expression level may be insufficient to induce a hybrid blood-lymphatic phenotype. Because *Vegfr3* is a direct target gene of PROX1(69), it is apparent that the postnatal CNS parenchyma establishes a microenvironment that prevents the upregulation of VEGFR3 expression in brain ECs. Detailed molecular mechanisms responsible for the suppression of LEC markers, such as VEGFR3*,* remain to be elucidated.

Despite the upregulation of LEC markers, including LYVE1, in ECs in brain tumors and AVMs, *Prox1*$^{iEC\text{-}OE}$ mutant ECs fail to differentiate into conventional LECs. These phenotypic differences suggest that the pathological microenvironments may provide additional signals that could induce the expression of the conventional LEC markers within the CNS parenchyma. The specific signals that alter the CNS non-permissive microenvironment for the development and growth of lymphatic vasculature are currently under investigation. Additionally, we should not discount the potential contribution of leptomeningeal LECs to the pathological brain parenchyma. While no

report currently supports the invasion of leptomeningeal LECs into the brain parenchyma in mammals, a transient invasion of non-lumenized LECs into the injured brain parenchyma has been observed in a zebrafish model (70, 71).

Endothelial *Prox1* expression leads to an increased vascular leakage and BBB disruption when induced during both embryonic and postnatal stages. These data suggest PROX1's inhibitory effects on barrier integrity. Indeed, the endothelial *Prox1* expression leads to decreased expression of TJ proteins such as CLDN5/Claudin-5 and ZO-1, along with the induction of PLVAP, a marker of high-permeability vasculature. Although our TEM analysis does not reveal discontinuous cell-cell junctions or fenestrations in *Prox1*$^{iEC\text{-}OE}$ mutant capillaries, cultured bEnd.3 cells expressing *Prox1* displayed discontinuous cell-cell junctions. While the RhoA/ROCK signaling pathway typically induces the formation of radial actin stress fibers, increased contractility, and the disruption of cell-cell junctions(72, 73), this is not the case in the cultured bEnd.3 cells expressing *Prox1.* Instead, the discontinuous cell-cell junctions in these cultured bEnd.3 cells are likely the result of a combination of actin fiber destabilization and relaxation, along with decreased expression of TJ proteins. *Prox1*$^{iEC\text{-}OE}$ mutants in vivo do not exhibit discontinuous cell-cell junctions or fenestrations in brain capillaries, probably due to pericyte coverage. In addition, our findings indicate that *Prox1* expression leads to the upregulation of transcytosis, as indicated by reduced expression of *Mfsd2a,* a lipid transporter that limits transcytosis in the BBB, and elevated expression of *caveolin-1/CAV1*, accompanied by an increased number of endothelial vesicles. Given that *Mfsd2a* expression is transcriptionally regulated by Wnt/ß-catenin

522 signaling in both in vivo(50, 51, 57, 61) and cultured bEnd.3 cells(51), PROX1 indirectly
523 upregulates transcytosis by downregulating Wnt/ß-catenin signaling. Overall, these
524 findings suggest that the endothelial *Prox1* expression leads to increased paracellular
525 and intercellular permeability of the BBB.
526
527 Considering prior research indicating that impaired EC ß-catenin signaling results in
528 increased paracellular and intercellular permeability of the BBB(46, 57-60), *Prox1*
529 expression impacts ß-catenin signaling, as evidenced by reduced expression of
530 *Ctnnb1/ß-catenin* and several effector and target genes including *Cldn5* and *Mfsd2a*.
531 Likewise, PROX1 appears to inhibit the promoter of *Ctnnb1/ß-catenin* or *Cldn5* gene in
532 ECs. How does PROX1 function as a transcriptional repressor in brain ECs? In
533 hepatocytes, PROX1 interacts with the class I histone deacetylase HDAC3 to
534 cooperatively repress gene transcription critical for maintaining lipid homeostasis(65). In
535 colorectal cancer cells, PROX1 interacts with HDAC1 in the nucleosome remodeling
536 and deacetylase (NuRD) complex to suppress Notch pathway(66). Indeed, HDAC2
537 mediates transcriptional regulation of BBB genes during BBB formation and
538 maintenance(74). Thus, it is plausible that PROX1 may interact with the class I histone
539 deacetylases such as HDAC2 to suppress the expression of *Ctnnb1/ß-catenin* or *Cldn5*
540 in brain ECs.
541
542 Our studies clearly demonstrate that while CNS establishes a non-permissive
543 microenvironment for the development and growth of conventional lymphatic
544 vasculature under physiological conditions, endothelial *Prox1* expression leads to

545 increased paracellular and intercellular permeability of the BBB. Despite the
546 upregulation of LEC markers and BBB disruption observed in CNS ECs in brain tumors
547 and AVMs, our genetic mouse models demonstrate that *Prox1* upregulation alone is
548 sufficient to trigger vascular malformations and BBB disruption in the CNS vasculature.
549 These findings indicate that tightly suppressing *Prox1* expression in CNS ECs may be
550 necessary to preserve BBB integrity and prevent lymphatic vasculature formation in the
551 CNS parenchyma. There are examples from non-CNS organs where *Prox1* suppression
552 is crucial for maintaining the segregation between blood and lymphatic vasculatures.
553 For instance, deficiency in *Folliculin (FLCN)*, a tumor suppressor gene responsible for
554 Birt-Hogg-Dubé (BHD) syndrome, leads to endothelial *Prox1* expression in veins,
555 causing improper connections between blood vessels and lymphatic vessels(38). In
556 zebrafish, the vascularization of the anal fin involves the transdifferentiation of pre-
557 existing lymphatic vessels into blood vessels, with *Sox17* playing a crucial role in
558 suppressing *Prox1* expression to facilitate the LEC-to-BEC transition(75).
559
560 Further studies are needed to elucidate the fundamental mechanisms underlying *Prox1*
561 suppression in brain ECs and the absence of lymphatic vessels within the CNS
562 parenchyma. In pathological conditions, dysregulation of *Prox1* expression could lead to
563 BBB alterations. Understanding the molecular links between *Prox1* regulation and
564 barrier disruption in disease states could facilitate the development of innovative
565 therapeutic strategies, either to enhance drug delivery to the brain or to restore BBB
566 function in the context of disease.
567

Methods

Sex as a biological variable.

In this study, sex was not considered as a biological variable in embryos and neonates.

Mice

The following mice (*Mus musculus*) were used in this study: C57BL/6J mice (The Jackson Laboratory), CD-1 mice (Charles River Laboratory), *Cadh5-BAC-Cre^{ERT2}* mice(39), and *Prox1-GFP BAC* mice(36). *Rosa26-LSL-Prox1* mice have been generated in the Mukouyama Lab and the NHLBI Transgenic Core. For timed mating, the morning of the vaginal plug was considered E0.5. The *Cre*-mediated excision was induced by administering 1.5-3 mg tamoxifen (Sigma-Aldrich) by intraperitoneal injection (I.P.) at embryonic day (E)13.5, and embryos were harvested at E16.5 for analysis. For postnatal analysis, tamoxifen injection was performed I.P. (0.5 mg) to each pup at postnatal day (P)7 and analysis was performed at P10.

Generation of *R26-LSL-Prox1* mice

The generation of *Rosa26-LSL-Prox1* mice was previously described(38). Briefly, a mouse *Prox1* coding sequence with 5' FLAG-tag was knocked into the mouse *Rosa26 locus* using the CRISPR/Cas9 method in the NHLBI Transgenic Core. The *R26-LoxP-STOP-LoxP-Prox1* construct was co-microinjected along with *Cas9* mRNA and sgRNA into the pronuclei of fertilized mouse eggs. After culturing the injected embryos overnight, embryos that had reached the 2-cell stage of development were implanted into the oviducts of pseudopregnant foster mothers.

591

592 **scRNA-seq analysis of publicly available datasets**

593 To evaluate lymphatic marker gene expressions, publicly available scRNA-seq datasets
594 were utilized. For glioblastoma, three datasets were retrieved from the Gene Expression
595 Omnibus (GEO) database under accession numbers GSE162631, GSE173278, and
596 GSE184357. For brain metastasis, dataset was downloaded at:
597 https://joycelab.shinyapps.io/braintime/. For AVMs, dataset was downloaded at:
598 https://adult-brain-vasc.cells.ucsc.edu. For the glioblastoma datasets, the endothelial
599 cell population was first subset from each dataset using R package Seurat. The three
600 endothelial datasets were then integrated using the integration method provided by the
601 Seurat package (76). Following integration, principal component analysis was
602 performed for dimensional reduction. Uniform Manifold Approximation and Projection
603 (UMAP) was then applied (dims = 1:30). For all three disease datasets (glioblastoma,
604 brain metastasis, and AVMs), UMAP plots, violin plots, and dot plots were visualized
605 using either scCustomize package in R (77) or Scanpy package in Python. To calculate
606 average gene expressions of lymphatic markers (*PROX1*, *LYVE1*, and *FLT4*) and
607 *PLVAP*, the AverageExpression function in Seurat was used.

608

609 **Histology and Immunofluorescence**

610 Embryos and neonates harvested from timed pregnancies (morning of plug designated
611 E0.5) were collected and washed in PBS and then fixed in 4% paraformaldehyde (PFA)
612 overnight at 4ºC with rotation. After washing in PBS, the fixed embryos and neonates
613 were equilibrated in a 15% to 30% sucrose gradient at 4°C overnight. The tissues were

614 embedded in Tissue-Tek O.C.T. Compound (Sakura). Cryosections were washed in
615 PBS, permeabilized with PBS-T (0.5% Triton X-100) for 5-10 minutes when needed,
616 and then blocked with 10% goat serum in PBS with 0.1% Triton X-100 or 1% bovine
617 serum albumin with 0.1% Triton X-100 for 1-2 hours at room temperature. Primary
618 antibodies with dilution 1:100-1:200 were incubated in blocking buffer at 4ºC overnight.
619 Fluorescence-conjugated secondary antibodies were used at the dilution of 1:300-1:500
620 in the blocking buffer, and sections were incubated with secondary antibodies for 1 hour
621 at room temperature. After washing in PBS, sections were mounted with ProLong glass
622 antifade mounting media (Thermo Fisher). Samples processed in similar manner,
623 excluding the use of primary antibodies, were employed as negative controls to verify
624 the staining's specificity in sections.
625
626 **Tissue clearing, whole-mount immunostaining, and confocal imaging.**
627 CUBIC method was used for tissue clearing as previously described(78). Briefly, after
628 washing the fixed tissues in PBS, the tissues were incubated with CUBIC reagent-1 (25
629 wt% urea, 25 wt% *N,N,N',N'*-tetrakis(2-hydroxypropyl) ethylenediamine, and 15% (v/v)
630 Triton X-100) for 1-2 days at room temperature with rotation. The tissues were blocked
631 with 10% goat serum in PBS with 0.1% Triton X-100 or 1% bovine serum albumin with
632 0.1% Triton X-100 for 12-24 hours. Primary (1:300) and secondary antibodies (1:500)
633 were diluted in the blocking buffer and all washes were performed in PBS-T (0.05%
634 Triton X-100 in PBS) with rotation. After whole-mount immunostaining, the tissues were
635 balanced with sucrose (20%) and incubation was performed with CUBIC reagent-2 (50
636 wt% sucrose, 25 wt% urea, 10 wt% 2,2′,2″-nitrilotriethanol, and 0.1% (v/v) Triton X-100)

637 at room temperature with rotation in the dark for 1 day. Cubic reagent-2 was used as
638 mounting medium for the confocal acquisition. All confocal microscopy was carried out
639 on a Leica TCS SP5 microscope. Optical z-stack projections were generated with FIJI
640 or Imaris software using a maximal intensity algorithm.
641
642 **Flow cytometry**
643 Embryonic or postnatal brains were isolated in cold HBSS medium (Thermo Fisher).
644 The brain tissues were minced into small pieces and digestion solution (0.05% DNase I,
645 0.1% collagenase, 0.3% dispase, in Leibovitz's L-15 medium (Thermo Fisher) was
646 incubated at 37ºC for 45 minutes with agitation every 5-10 minutes. After dissociation,
647 remaining clumps of cells were filtered through 70-µm filters and washed with cold
648 FACS buffer (1% BSA, 0.1 M HEPES, 1x Pen-Strep, 0.025% DNase I, in L15 medium).
649 Cells were centrifuged and resuspended in cold FACs buffer. Negative selection with
650 magnet beads was performed to eliminate erythrocytes and myeloid cells. Briefly, cells
651 were incubated with mouse anti-Ter119 (eBioscience, 1:100), mouse anti-CD45
652 (Biolegend, 1:100) for 30 minutes on ice. After washing with FACS buffer, cells were
653 incubated with anti-rat IgG conjugated magnetic beads for 30 minutes. Negative
654 selection was performed using a magnetic stand with 2 minutes of incubation per
655 sample. Final samples were stained with the following antibody mix. All flow cytometry
656 analyses were done on BD LSR Fortessa equipped with Diva Software. Cell sorting was
657 performed using BD FACSMelody, BD FACSymphony or BD FACSAria Fusion.
658 Unstained samples, single-color staining, and fluorescence minus one (FMO) were
659 used to establish the proper compensation and gating. In all samples, debris, blood

cells and myeloid cells were gated out by DAPI, Ter119, and CD45 staining. Antibodies used for cytometry are listed: rat monoclonal anti-Ter119-BV785 (Biolegend, 1;100), rat monoclonal anti-CD45-BV785 (Biolegend, 1:100), rat monoclonal anti-CD31-PECy7 (eBioscience, 1:100), rat monoclonal anti-CD140b-APC (eBioscience, 1:100), rat monoclonal anti-NG2 AF488 (Millipore sigma, 1:100), rat monoclonal anti-LYVE-1-PE (MBL, 1:100). Data was analyzed using FlowJo software (BD biosciences).

Quantitative real time PCR

mRNA was extracted from embryonic, postnatal brain, and skin ECs using PicoPure RNA Isolation Kit (Thermo Fisher), according to the manufacturer's instructions. The mRNA was converted to cDNA using SuperScript III Reverse Transcriptase (Thermo Fisher). Quantitative real time (qRT)-PCR was performed in triplicate with Power SYBR™ Green Master Mix 2x (Roche). Relative quantification of each transcript was obtained by normalizing against *GADPH* transcript abundance. The general cycling conditions were as follows: one initial hold for 3 minutes at 95ºC, followed by 40x cycles of 10-sec denaturation (95ºC) and 45 seconds of annealing/extension at 60ºC. The sequences of oligonucleotides for qRT- PCR are listed in Supplementary Methods:

Blood-brain barrier permeability assay

Embryos were harvested at E16.5. Once the placenta and yolk sac were removed, 3kDa Dextran Texas-red (Invitrogen) was injected into the left ventricle of the heart (10µg in PBS) using a mouth pipette and glass capillaries. Injected embryos were incubated in HBSS medium for 5 min at room temperature, followed by fixation in 10%

PFA/PBS for 2 hours at room temperature and rotation. After fixation, the embryos were washed three times with PBS, and then were equilibrated in a 15% to 30% sucrose gradient at 4°C overnight. The following day, tissues were embedded in Tissue-Tek O.C.T. Compound (Sakura) for cryosections or tissue-clearing and whole-mount immunostaining. Those embryos where the heart was not pumping correctly were not considered for analysis.

Neonates were harvested at P10 and injected intraperitoneally with 250µg 3kDa Dextran Texas-Red (Invitrogen) per 20g mouse or 100µg 1kDa Cadaverine (Thermo Fisher) per 20g mouse, as previously reported(79). After 2 hours, pups were euthanized, and brain tissues were harvested for fixation and posterior analysis. Leakage was determined by making a mask of the vasculature area using the PECAM1 channel, then assessing the dextran or cadaverine signal outside of the vasculature.

Cell culture

Commercially available bEnd.3 cells (ATCC) were cultured in DMEM complete (ATCC) supplemented with 10% FBS, and 10 mM Penicillin/Streptomycin. Commercially available primary RBMVECs (Cell applications) were cultured in rat brain endothelial cell growth medium (Sigma) supplemented with 10 mM Penicillin/Streptomycin, according to the manufacturer's instructions. All cells were maintained at 37°C and 5% CO_2.

For lentivirus infection, cells were seeded onto 12-well glass chamber slides (Ibidi) coated with 10 µg/ml fibronectin (Millipore-Sigma) or attachment factor solution (Cell application). Once cells reached ~60-70% confluency, cell medium was removed and fresh cell medium containing 1 mg/ml polybrene (Vector builder) and lentivirus expressing *Gfp* or *Prox1* was added (MOI 5-10). For each experiment, three separate plates were seeded with cells, one with no lentivirus, one with *Gfp*-lentivirus, and one with *Prox1*-lentivirus. Two days after the lentivirus infection, the cell medium was changed, and cells were fixed with 4% PFA for 10 minutes at RT when reached a confluent monolayer. Immunostaining was performed as described above. Cells were permeabilized with 0.1% Triton X-100 for 10 minutes at RT followed by blocking with BSA buffer for 1-2 hours at room temperature. Primary antibodies were incubated overnight at 4°C and secondary antibodies (1:400) the following day for 1-2 hours at room temperature. After the washing steps, Ibidi chambers were removed, and slides were mounted normally using ProLong mounting media (Thermo Fisher).

The following primary antibodies were used in cell culture: Goat anti-Prox1 (R&D, 1:100), mouse anti-Claudin-5 (Invitrogen, 1:100), rabbit anti-ZO-1 (Proteintech, 1:300), goat anti-GFP (Abcam 1:200), rabbit anti-pMLC2 (Cell signaling, 1:200), and Alexa Fluor 568 Phalloidin (Invitrogen, 1:500). RBMVECs at passages 3-5 were used for experiments. All confocal microscopy was carried out on a Leica TCS SP5 microscope using a 63x oil objective.

Transmission Electron Microscopy

Postnatal brains were harvested and fixed by immersion in a 0.1M sodium cacodylate-buffered mixture (2.5% glutaraldehyde and 4% PFA) for 2 hours at RT followed by overnight incubation in 4% PFA at 4°C. The next day, tissues were washed two times in 0.1M sodium cacodylate buffer and then cut in 200 μm-thick free-floating sections using a vibratome. Sections were then post-fixed in 2% osmium tetroxide and 1.5% potassium ferrocyanide and stained overnight in 1% UA. The following day samples were dehydrated in graded ethanol series and infiltrated with resin (Embed-812) and baked at 60ºC for 48 hours. Ultrathin sections (65-70 nm) were cut on an ultramicrotome (Leica EM UC7), and digital micrographs were acquired with a JOEL JEM 1200 EXII (80 kV) equipped with an AMT XR-60 digital camera.

Quantification and Statistical Analysis

All data were collected from at least three independent experiments as indicated. The actual number of independent biological replicates are specified, wherever applicable, in the relevant figure legends. Statistical analyses were performed using Prism (GraphPad v9.0). Data are presented as mean values ±SEM. The Shapiro-Wilk test was used to check the normality of data distribution. When the normality assumption was met, unpaired t-test was applied to assess the significance. For all the images included across the manuscript, the most representative examples reflecting the typical phenotype were selected.

Study approval

All animal procedures were approved by the National Heart, Lung, and Blood Institute (NHLBI) Animal Care and Use Committee in accordance with NIH research guidelines for the care and use of laboratory animals.

Data availability

All data in the manuscript is included in the Support Data Values file.

ACKNOWLEGMENTS

Thanks to P. Dagur, M. Lopez-Ocasio, and K. Keyvanfar of the NHLBI Flow Cytometry Core for FACS assistance; Z. Syed of the NHLBI Electron Microscopy Core for TEM assistance; T. Markowitz and N. Redekar of Research Technology Branch in the National Institute of Allergy and Infectious Diseases (NIAID) for ChIP-seq data analysis; T. Clark and the staff of NIH Bldg50 animal facility for assistance with mouse breeding and care. Thanks also to C. Conrad of the Developmental Therapeutics and Pharmacology Unit in National Institute of Neurological Disorders and Stroke (NINDS) for sharing reagents; C. Waterman, R. Fischer, A. Pasapera in the Laboratory of Cell and Tissue Morphodynamics (NHLBI), and V. Bautch and D. Buglak (University of North Carolina) for sharing reagents and valuable discussion. Thanks also to K. Gill for laboratory management and technical support, V. Sam for administrative assistance, and members of the Laboratory of Stem Cell and Neuro-Vascular Biology for technical help and thoughtful discussion. S. González-Hernández is supported by the NHLBI Lenfant Biomedical Fellowship. This work was also supported by the Intramural Research Program of the NHLBI, NIH (HL006115-14 to Y-S Mukouyama).

Author contributions

S. G-H conducted all the experiments, and also contributed to the conceptualization, writing and editing of the manuscript. Y. S., C. L., W. L., and C. L were responsible for generating and conducting the primary characterization of *R26-LSL-Prox1* mice. S. J. provided valuable reagents. Y. K. provided *Cdh5-Cre*^{ERT2} mice. Y-S. M. contributed through project supervision, discussion, and writing and editing of the manuscript.

REFERENCES

1. Daneman R, and Prat A. The blood-brain barrier. *Cold Spring Harb Perspect Biol.* 2015;7(1):a020412.
2. Zhao Z, Nelson AR, Betsholtz C, and Zlokovic BV. Establishment and Dysfunction of the Blood-Brain Barrier. *Cell.* 2015;163(5):1064-78.
3. Obermeier B, Daneman R, and Ransohoff RM. Development, maintenance and disruption of the blood-brain barrier. *Nat Med.* 2013;19(12):1584-96.
4. Langen UH, Ayloo S, and Gu C. Development and Cell Biology of the Blood-Brain Barrier. *Annu Rev Cell Dev Biol.* 2019;35:591-613.
5. Rattner A, Wang Y, and Nathans J. Signaling Pathways in Neurovascular Development. *Annu Rev Neurosci.* 2022;45:87-108.
6. Murphy JB, and Sturm E. Conditions Determining the Transplantability of Tissues in the Brain. *J Exp Med.* 1923;38(2):183-97.
7. Medawar PB. Immunity to homologous grafted skin; the fate of skin homografts transplanted to the brain, to subcutaneous tissue, and to the anterior chamber of the eye. *Br J Exp Pathol.* 1948;29(1):58-69.
8. Shirai Y. On the transplantation of the rat sarcoma in adult heterogenous animals. *Jap Med World.* 1921;1.
9. Wigle JT, and Oliver G. Prox1 function is required for the development of the murine lymphatic system. *Cell.* 1999;98(6):769-78.
10. Francois M, Caprini A, Hosking B, Orsenigo F, Wilhelm D, Browne C, et al. Sox18 induces development of the lymphatic vasculature in mice. *Nature.* 2008;456(7222):643-69.
11. Hong YK, Harvey N, Noh YH, Schacht V, Hirakawa S, Detmar M, et al. Prox1 is a master control gene in the program specifying lymphatic endothelial cell fate. *Dev Dynam.* 2002;225(3):351-7.
12. Petrova TV, Makinen T, Makela TP, Saarela J, Virtanen I, Ferrell RE, et al. Lymphatic endothelial reprogramming of vascular endothelial cells by the Prox-1 homeobox transcription factor. *EMBO J.* 2002;21(17):4593-9.
13. Johnson NC, Dillard ME, Baluk P, McDonald DM, Harvey NL, Frase SL, et al. Lymphatic endothelial cell identity is reversible and its maintenance requires Prox1 activity. *Genes Dev.* 2008;22(23):3282-91.
14. Kim H, Nguyen VP, Petrova TV, Cruz M, Alitalo K, and Dumont DJ. Embryonic vascular endothelial cells are malleable to reprogramming via Prox1 to a lymphatic gene signature. *Bmc Dev Biol.* 2010;10:72.
15. Kim H, Cruz M, Bourdeau A, and Dumont DJ. Cell-cell interactions influence vascular reprogramming by Prox1 during embryonic development. *Plos One.* 2013;8(1):e52197.
16. Louveau A, Smirnov I, Keyes TJ, Eccles JD, Rouhani SJ, Peske JD, et al. Structural and functional features of central nervous system lymphatic vessels. *Nature.* 2015;523(7560):337-41.
17. Aspelund A, Antila S, Proulx ST, Karlsen TV, Karaman S, Detmar M, et al. A dural lymphatic vascular system that drains brain interstitial fluid and macromolecules. *J Exp Med.* 2015;212(7):991-9.
18. Izen RM, Yamazaki T, Nishinaka-Arai Y, Hong YK, and Mukouyama YS. Postnatal development of lymphatic vasculature in the brain meninges. *Dev Dynam.* 2018;247(5):741-53.
19. Jacob L, de Brito Neto J, Lenck S, Corcy C, Benbelkacem F, Geraldo LH, et al. Conserved meningeal lymphatic drainage circuits in mice and humans. *J Exp Med.* 2022;219(8).

20. Bower NI, Koltowska K, Pichol-Thievend C, Virshup I, Paterson S, Lagendijk AK, et al. Mural lymphatic endothelial cells regulate meningeal angiogenesis in the zebrafish. *Nat Neurosci.* 2017;20(6):774-83.
21. van Lessen M, Shibata-Germanos S, van Impel A, Hawkins TA, Rihel J, and Schulte-Merker S. Intracellular uptake of macromolecules by brain lymphatic endothelial cells during zebrafish embryonic development. *Elife.* 2017;6.
22. Venero Galanternik M, Castranova D, Gore AV, Blewett NH, Jung HM, Stratman AN, et al. A novel perivascular cell population in the zebrafish brain. *Elife.* 2017;6.
23. Castranova D, Samasa B, Venero Galanternik M, Jung HM, Pham VN, and Weinstein BM. Live Imaging of Intracranial Lymphatics in the Zebrafish. *Circ Res.* 2021;128(1):42-58.
24. Shibata-Germanos S, Goodman JR, Grieg A, Trivedi CA, Benson BC, Foti SC, et al. Structural and functional conservation of non-lumenized lymphatic endothelial cells in the mammalian leptomeninges. *Acta Neuropathol.* 2020;139(2):383-401.
25. Meng FW, Jing XN, Song GH, Jie LL, and Shen FF. Prox1 induces new lymphatic vessel formation and promotes nerve reconstruction in a mouse model of sciatic nerve crush injury. *J Anat.* 2020;237(5):933-40.
26. Shoemaker LD, Fuentes LF, Santiago SM, Allen BM, Cook DJ, Steinberg GK, et al. Human brain arteriovenous malformations express lymphatic-associated genes. *Ann Clin Transl Neurol.* 2014;1(12):982-95.
27. Zhao L, Qiu Z, Yang Z, Xu L, Pearce TM, Wu Q, et al. Lymphatic endothelial-like cells promote glioblastoma stem cell growth through cytokine-driven cholesterol metabolism. *Nat Cancer.* 2024;5(1):147-66.
28. Liu I, Jiang L, Samuelsson ER, Marco Salas S, Beck A, Hack OA, et al. The landscape of tumor cell states and spatial organization in H3-K27M mutant diffuse midline glioma across age and location. *Nat Genet.* 2022;54(12):1881-94.
29. LeBlanc VG, Trinh DL, Aslanpour S, Hughes M, Livingstone D, Jin D, et al. Single-cell landscapes of primary glioblastomas and matched explants and cell lines show variable retention of inter- and intratumor heterogeneity. *Cancer Cell.* 2022;40(4):379-92 e9.
30. Xie Y, He L, Lugano R, Zhang Y, Cao H, He Q, et al. Key molecular alterations in endothelial cells in human glioblastoma uncovered through single-cell RNA sequencing. *JCI Insight.* 2021;6(15).
31. Bejarano L, Kauzlaric A, Lamprou E, Lourenco J, Fournier N, Ballabio M, et al. Interrogation of endothelial and mural cells in brain metastasis reveals key immune-regulatory mechanisms. *Cancer Cell.* 2024;42(3):378-95 e10.
32. Winkler EA, Kim CN, Ross JM, Garcia JH, Gil E, Oh I, et al. A single-cell atlas of the normal and malformed human brain vasculature. *Science.* 2022;375(6584):eabi7377.
33. Stan RV, Kubitza M, and Palade GE. PV-1 is a component of the fenestral and stomatal diaphragms in fenestrated endothelia. *Proc Natl Acad Sci U S A.* 1999;96(23):13203-7.
34. Stan RV, Tkachenko E, and Niesman IR. PV1 is a key structural component for the formation of the stomatal and fenestral diaphragms. *Mol Biol Cell.* 2004;15(8):3615-30.
35. Stan RV, Tse D, Deharvengt SJ, Smits NC, Xu Y, Luciano MR, et al. The diaphragms of fenestrated endothelia: gatekeepers of vascular permeability and blood composition. *Dev Cell.* 2012;23(6):1203-18.
36. Choi I, Chung HK, Ramu S, Lee HN, Kim KE, Lee S, et al. Visualization of lymphatic vessels by Prox1-promoter directed GFP reporter in a bacterial artificial chromosome-based transgenic mouse. *Blood.* 2011;117(1):362-5.
37. Lavado A, Lagutin OV, Chow LM, Baker SJ, and Oliver G. Prox1 is required for granule cell maturation and intermediate progenitor maintenance during brain neurogenesis. *PLoS Biol.* 2010;8(8).

38. Tai-Nagara I, Hasumi Y, Kusumoto D, Hasumi H, Okabe K, Ando T, et al. Blood and lymphatic systems are segregated by the FLCN tumor suppressor. *Nat Commun.* 2020;11(1):6314.
39. Okabe K, Kobayashi S, Yamada T, Kurihara T, Tai-Nagara I, Miyamoto T, et al. Neurons limit angiogenesis by titrating VEGF in retina. *Cell.* 2014;159(3):584-96.
40. Ben-Zvi A, Lacoste B, Kur E, Andreone BJ, Mayshar Y, Yan H, et al. Mfsd2a is critical for the formation and function of the blood-brain barrier. *Nature.* 2014;509(7501):507-11.
41. Klotz L, Norman S, Vieira JM, Masters M, Rohling M, Dube KN, et al. Cardiac lymphatics are heterogeneous in origin and respond to injury. *Nature.* 2015;522(7554):62-7.
42. Aspelund A, Tammela T, Antila S, Nurmi H, Leppanen VM, Zarkada G, et al. The Schlemm's canal is a VEGF-C/VEGFR-3-responsive lymphatic-like vessel. *J Clin Invest.* 2014;124(9):3975-86.
43. Park DY, Lee J, Park I, Choi D, Lee S, Song S, et al. Lymphatic regulator PROX1 determines Schlemm's canal integrity and identity. *J Clin Invest.* 2014;124(9):3960-74.
44. Truong TN, Li H, Hong YK, and Chen L. Novel characterization and live imaging of Schlemm's canal expressing Prox-1. *Plos One.* 2014;9(5):e98245.
45. Hallmann R, Mayer DN, Berg EL, Broermann R, and Butcher EC. Novel mouse endothelial cell surface marker is suppressed during differentiation of the blood brain barrier. *Dev Dyn.* 1995;202(4):325-32.
46. Zhou Y, Wang Y, Tischfield M, Williams J, Smallwood PM, Rattner A, et al. Canonical WNT signaling components in vascular development and barrier formation. *J Clin Invest.* 2014;124(9):3825-46.
47. Lugano R, Vemuri K, Barbera S, Orlandini M, Dejana E, Claesson-Welsh L, et al. CD93 maintains endothelial barrier function by limiting the phosphorylation and turnover of VE-cadherin. *Faseb J.* 2023;37(4):e22894.
48. Cottarelli A, Corada M, Beznoussenko GV, Mironov AA, Globisch MA, Biswas S, et al. Fgfbp1 promotes blood-brain barrier development by regulating collagen IV deposition and maintaining Wnt/beta-catenin signaling. *Development.* 2020;147(16).
49. Andreone BJ, Chow BW, Tata A, Lacoste B, Ben-Zvi A, Bullock K, et al. Blood-Brain Barrier Permeability Is Regulated by Lipid Transport-Dependent Suppression of Caveolae-Mediated Transcytosis. *Neuron.* 2017;94(3):581-94 e5.
50. Wang Z, Liu CH, Huang S, Fu Z, Tomita Y, Britton WR, et al. Wnt signaling activates MFSD2A to suppress vascular endothelial transcytosis and maintain blood-retinal barrier. *Sci Adv.* 2020;6(35):eaba7457.
51. Cui Y, Wang Y, Song X, Ning H, Zhang Y, Teng Y, et al. Brain endothelial PTEN/AKT/NEDD4-2/MFSD2A axis regulates blood-brain barrier permeability. *Cell Rep.* 2021;36(1):109327.
52. Armulik A, Genove G, Mae M, Nisancioglu MH, Wallgard E, Niaudet C, et al. Pericytes regulate the blood-brain barrier. *Nature.* 2010;468(7323):557-61.
53. Daneman R, Zhou L, Kebede AA, and Barres BA. Pericytes are required for blood-brain barrier integrity during embryogenesis. *Nature.* 2010;468(7323):562-6.
54. Daneman R, Agalliu D, Zhou L, Kuhnert F, Kuo CJ, and Barres BA. Wnt/beta-catenin signaling is required for CNS, but not non-CNS, angiogenesis. *Proc Natl Acad Sci U S A.* 2009;106(2):641-6.
55. Wang Y, Cho C, Williams J, Smallwood PM, Zhang C, Junge HJ, et al. Interplay of the Norrin and Wnt7a/Wnt7b signaling systems in blood-brain barrier and blood-retina barrier development and maintenance. *Proc Natl Acad Sci U S A.* 2018;115(50):E11827-E36.
56. Zhang Y, Chen K, Sloan SA, Bennett ML, Scholze AR, O'Keeffe S, et al. An RNA-sequencing transcriptome and splicing database of glia, neurons, and vascular cells of the cerebral cortex. *J Neurosci.* 2014;34(36):11929-47.

57. Hussain B, Fang C, Huang X, Feng Z, Yao Y, Wang Y, et al. Endothelial beta-Catenin Deficiency Causes Blood-Brain Barrier Breakdown via Enhancing the Paracellular and Transcellular Permeability. *Front Mol Neurosci.* 2022;15:895429.
58. Liebner S, Corada M, Bangsow T, Babbage J, Taddei A, Czupalla CJ, et al. Wnt/beta-catenin signaling controls development of the blood-brain barrier. *J Cell Biol.* 2008;183(3):409-17.
59. Tran KA, Zhang X, Predescu D, Huang X, Machado RF, Gothert JR, et al. Endothelial beta-Catenin Signaling Is Required for Maintaining Adult Blood-Brain Barrier Integrity and Central Nervous System Homeostasis. *Circulation.* 2016;133(2):177-86.
60. Wang Y, Rattner A, Zhou Y, Williams J, Smallwood PM, and Nathans J. Norrin/Frizzled4 signaling in retinal vascular development and blood brain barrier plasticity. *Cell.* 2012;151(6):1332-44.
61. Sabbagh MF, Heng JS, Luo C, Castanon RG, Nery JR, Rattner A, et al. Transcriptional and epigenomic landscapes of CNS and non-CNS vascular endothelial cells. *Elife.* 2018;7.
62. Sato Y, Uchida Y, Hu J, Young-Pearse TL, Niikura T, and Mukouyama YS. Soluble APP functions as a vascular niche signal that controls adult neural stem cell number. *Development.* 2017;144(15):2730-6.
63. Dorland YL, and Huveneers S. Cell-cell junctional mechanotransduction in endothelial remodeling. *Cell Mol Life Sci.* 2017;74(2):279-92.
64. Kaltezioti V, Antoniou D, Stergiopoulos A, Rozani I, Rohrer H, and Politis PK. Prox1 regulates Olig2 expression to modulate binary fate decisions in spinal cord neurons. *J Neurosci.* 2014;34(47):15816-31.
65. Armour SM, Remsberg JR, Damle M, Sidoli S, Ho WY, Li Z, et al. An HDAC3-PROX1 corepressor module acts on HNF4alpha to control hepatic triglycerides. *Nat Commun.* 2017;8(1):549.
66. Hogstrom J, Heino S, Kallio P, Lahde M, Leppanen VM, Balboa D, et al. Transcription Factor PROX1 Suppresses Notch Pathway Activation via the Nucleosome Remodeling and Deacetylase Complex in Colorectal Cancer Stem-like Cells. *Cancer Res.* 2018;78(20):5820-32.
67. Gramolelli S, Cheng J, Martinez-Corral I, Vaha-Koskela M, Elbasani E, Kaivanto E, et al. PROX1 is a transcriptional regulator of MMP14. *Sci Rep.* 2018;8(1):9531.
68. Wong BW, Wang X, Zecchin A, Thienpont B, Cornelissen I, Kalucka J, et al. The role of fatty acid beta-oxidation in lymphangiogenesis. *Nature.* 2017;542(7639):49-54.
69. Srinivasan RS, Escobedo N, Yang Y, Interiano A, Dillard ME, Finkelstein D, et al. The Prox1-Vegfr3 feedback loop maintains the identity and the number of lymphatic endothelial cell progenitors. *Genes Dev.* 2014;28(19):2175-87.
70. Chen J, Li X, Ni R, Chen Q, Yang Q, He J, et al. Acute brain vascular regeneration occurs via lymphatic transdifferentiation. *Dev Cell.* 2021;56(22):3115-27 e6.
71. Chen J, He J, Ni R, Yang Q, Zhang Y, and Luo L. Cerebrovascular Injuries Induce Lymphatic Invasion into Brain Parenchyma to Guide Vascular Regeneration in Zebrafish. *Dev Cell.* 2019;49(5):697-710 e5.
72. Waschke J, Drenckhahn D, Adamson RH, Barth H, and Curry FE. cAMP protects endothelial barrier functions by preventing Rac-1 inhibition. *Am J Physiol Heart Circ Physiol.* 2004;287(6):H2427-33.
73. Waschke J, Baumgartner W, Adamson RH, Zeng M, Aktories K, Barth H, et al. Requirement of Rac activity for maintenance of capillary endothelial barrier properties. *Am J Physiol Heart Circ Physiol.* 2004;286(1):H394-401.
74. Sadanandan J, Thomas S, Mathew IE, Huang Z, Blackburn SL, Tandon N, et al. Establishing And Maintaining The Blood-Brain Barrier: Epigenetic And Signaling Determinants. *bioRxiv.* 2023:2022.11.29.516809.

75. Das RN, Tevet Y, Safriel S, Han Y, Moshe N, Lambiase G, et al. Generation of specialized blood vessels via lymphatic transdifferentiation. *Nature.* 2022;606(7914):570-5.
76. Stuart T, Butler A, Hoffman P, Hafemeister C, Papalexi E, Mauck WM, 3rd, et al. Comprehensive Integration of Single-Cell Data. *Cell.* 2019;177(7):1888-902 e21.
77. Marsh S, , Salmon M, , and Hoffman P. scCustomize: an R package for custom visualization & analyses of single cell sequencing https://samuel-marsh.github.io/scCustomize/ https://doi.org/10.5281/zenodo.5706430 2021.
78. Gonzalez-Hernandez S, Gomez MJ, Sanchez-Cabo F, Mendez-Ferrer S, Munoz-Canoves P, and Isern J. Sox17 Controls Emergence and Remodeling of Nestin-Expressing Coronary Vessels. *Circ Res.* 2020;127(11):e252-e70.
79. Boye K, Geraldo LH, Furtado J, Pibouin-Fragner L, Poulet M, Kim D, et al. Endothelial Unc5B controls blood-brain barrier integrity. *Nat Commun.* 2022;13(1):1169.

Figure 1

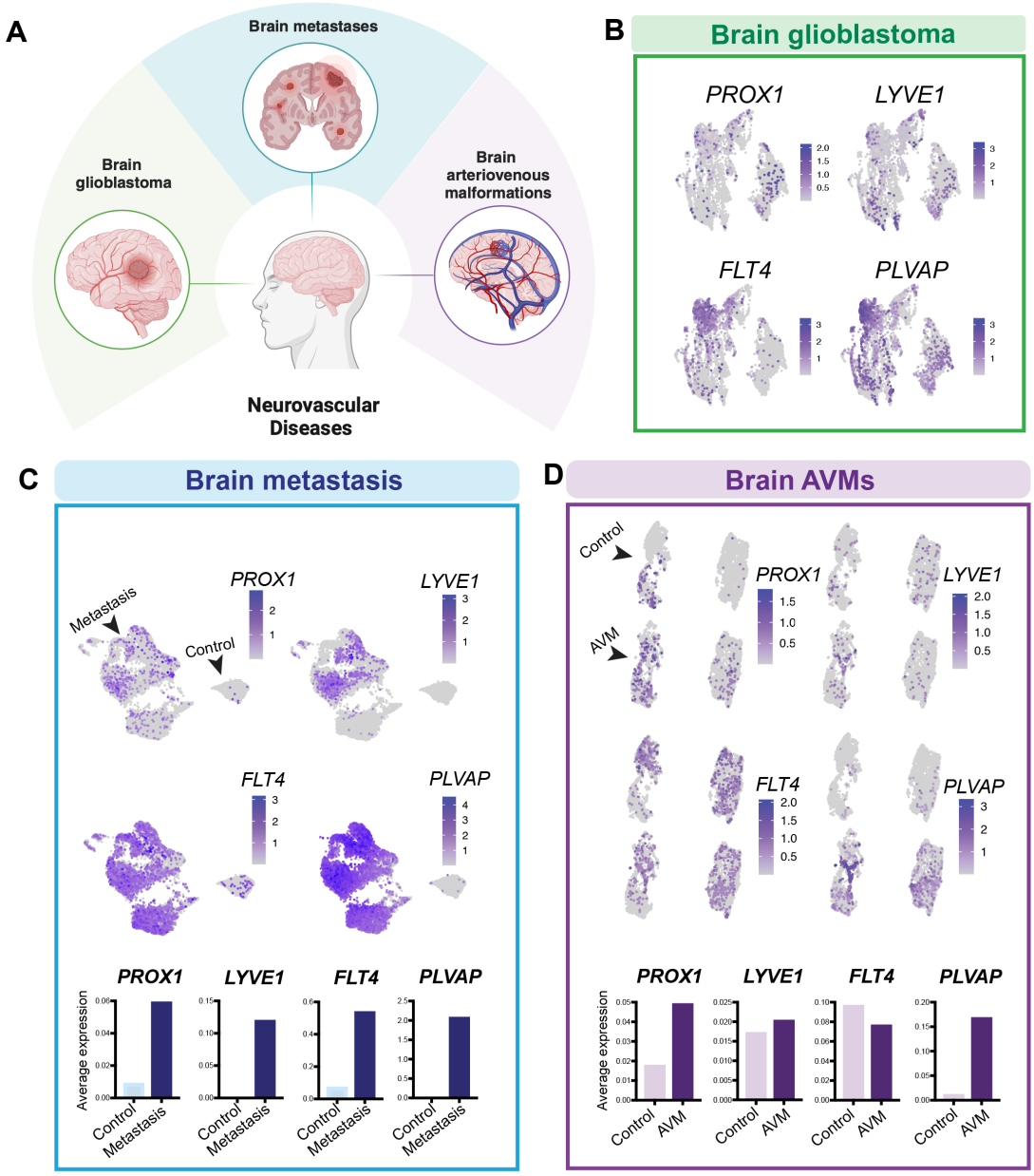

Figure 1. LEC markers are upregulated in ECs within human brain tumors and vascular malformations.
(A) Schematic representation of human brain vascular diseases for publicly available single-cell RNA-seq (scRNA-seq) data analysis. scRNA-seq datasets for human glioblastoma (28-30), tumor metastasis (31) and brain arteriovenous malformations (AVMs) (32) were used. **(B)** UMAP plots of scRNA-seq data from glioblastoma datasets display endothelial cell (EC) clusters expressing LEC markers, including PROX1, LYVE1, and FLT4, along with the vascular permeability marker PLVAP. **(C)** UMAP plots and average gene expression charts of scRNA-seq data of control and metastatic brain tumor datasets display EC clusters expressing LEC markers, including PROX1, LYVE1, and FLT4, along with the vascular permeability marker PLVAP. **(D)** UMAP plots and average gene expression charts of scRNA-seq data of control and AVM datasets display EC clusters expressing LEC markers, including PROX1, LYVE1, and FLT4, along with the vascular permeability marker PLVAP.

Figue 2

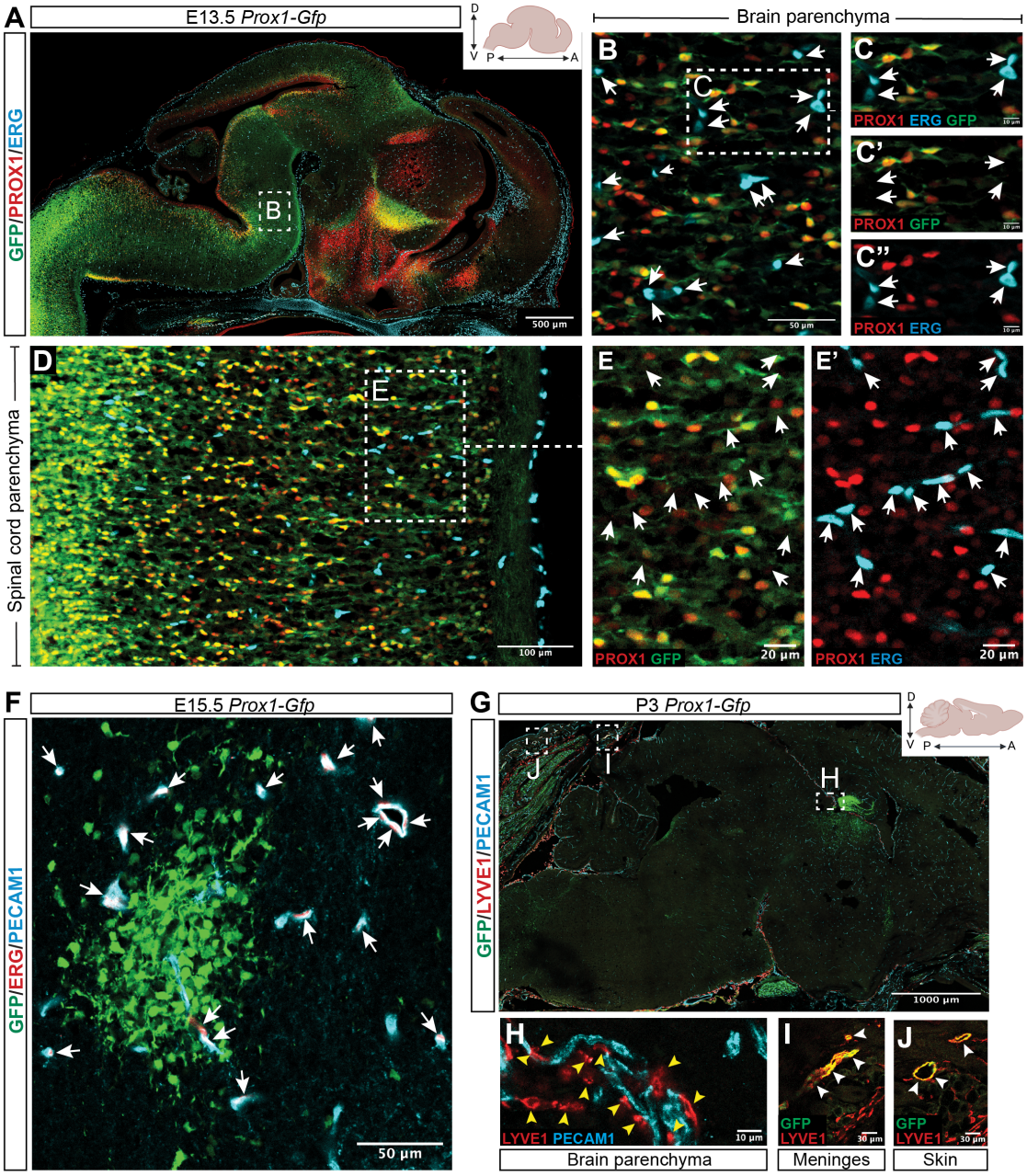

Figure 2. No temporal expression of Prox1 in the CNS vasculature.
(A-E) A sagittal view of the brain (A-C) and spinal cord (D-E) parenchyma in E13.5 *Prox1-Gfp BAC* transgenic reporter embryos labeled with PROX1 (red) and ERG (cyan). The boxed regions in (A, B, and D) are magnified in (B, C-C'', and E-E'), respectively. Arrows indicate ERG+ EC nuclei in (B, C-C'' and E-E'). These cells do not co-localize with PROX1 and *Prox1-GFP*. Scale bars: 500 µm in (A), 100 µm in (D), 50 µm in (B), 20 µm in (E-E'), and 10 µm in (C-C''). **(F)** Brain parenchyma of E15.5 *Prox1-Gfp* embryos labeled with PECAM1 (cyan) and ERG (red). Arrows indicate ERG+/PECAM1+ ECs. These cells do not co-localize with *Prox1-GFP*. Scale bar: 50 µm. **(G-J)** A sagittal view of a postnatal brain section (P3) labeled with LYVE1 (red) and PECAM1 (cyan). The boxed regions in (G) are magnified in (H-J). Yellow arrowheads in (H) indicate LYVE1+/PECAM1-/Prox1-GFP-macrophages. Arrowheads in (I and J) indicate PECAM1+/LYVE1+/Prox1-GFP+ lymphatic vessels in the meninges and skin, respectively. Scale bars: 1000 µm in (G), 30 µm in (I and J), and 10 µm in (H). The illustrations are created with BioRender.com.

Figure 3

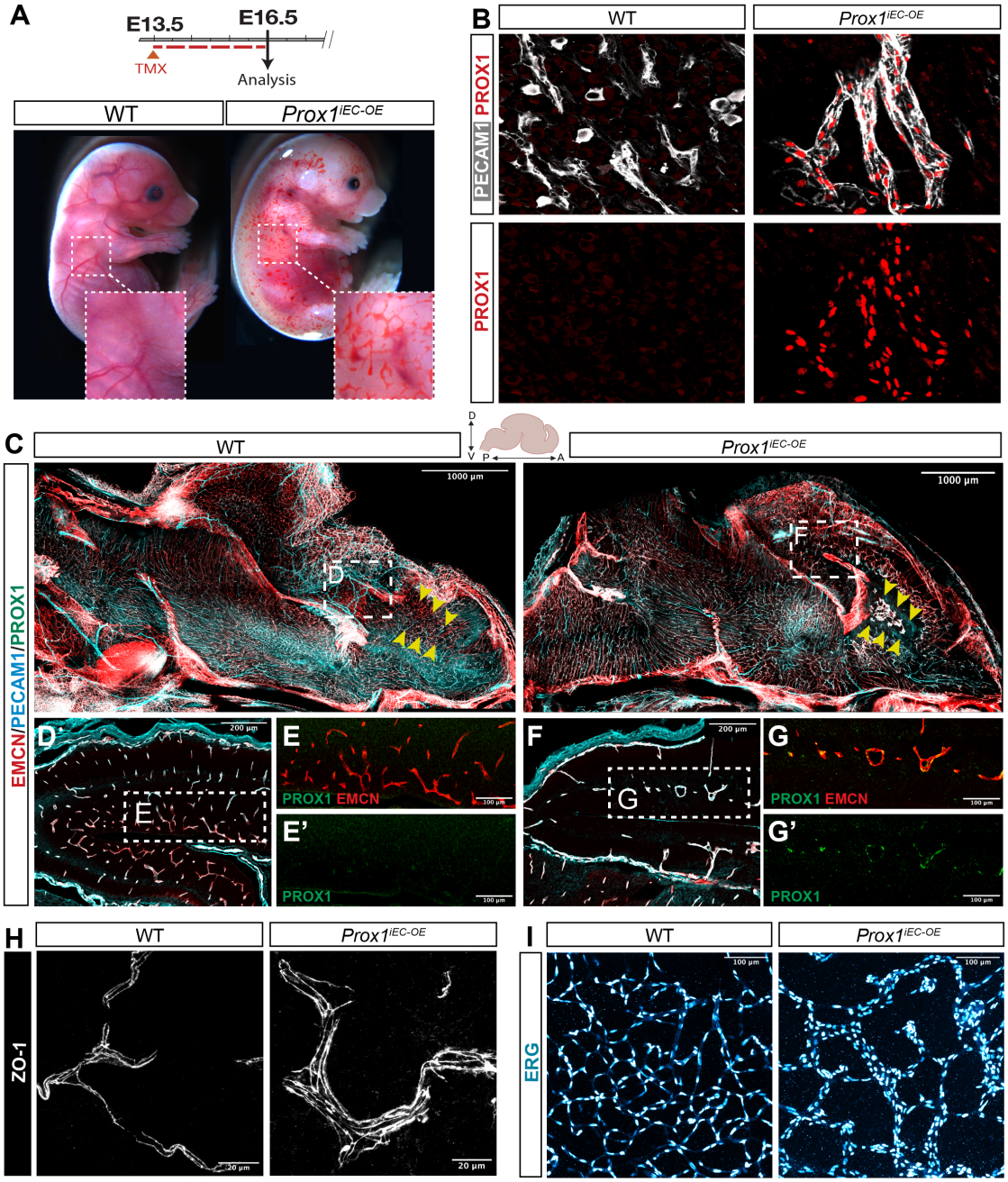

Figure 3. Endothelial *Prox1* expression induces vascular abnormalities in the developing CNS vasculature when induced during embryonic stages. **(A)** Diagram depicting EC-specific induction of *Prox1* expression at E13.5 and analysis of embryos at E16.5, and gross appearance of E16.5 *Prox1*$^{iEC\text{-}OE}$ mutant and their WT control littermate embryos. The boxed regions show blood-filled lymphatic vessels in the mutants when compared to control littermates. **(B)** Section immunostaining of E16.5 *Prox1*$^{iEC\text{-}OE}$ mutant and their WT control littermate brains with antibodies to PROX1 (red) and PECAM1 (grey). Prox1 expression, detected with anti-PROX1 antibody (red), is significantly induced in PECAM1+ brain vasculature (grey) of E16.5 *Prox1*$^{iEC\text{-}OE}$ mutants compared to their WT control littermates. **(C-G)** A sagittal view of whole-mount immunostaining of E16.5 *Prox1*$^{iEC\text{-}OE}$ mutant and their WT control littermate brains labeled with EMCN (red), PECAM1 (cyan) and PROX1 (green). The boxed regions in (C) are magnified in (D) as WT control and (F) as *Prox1*$^{iEC\text{-}OE}$ mutant. The boxed regions in (D and F) are magnified in (E-E' and G-G'), respectively. Yellow arrowheads in (C) indicate cortical vasculature. *Prox1*$^{iEC\text{-}OE}$ mutants exhibited PROX1+/EMCN+ enlarged capillaries (F and G-G') in comparison to their WT control littermates (D and E-E'). Scale bars: 1000 µm in (C), 200 µm in (D and F), and 100 µm in (E-E' and G-G'). **(H-I)** Section immunostaining of E16.5 *Prox1*$^{iEC\text{-}OE}$ mutant and their WT control littermate brains with ZO-1 (H, grey) and ERG (I, hot cyan). *Prox1*$^{iEC\text{-}OE}$ mutants exhibited enlarged capillaries with an increased number of ECs in comparison to their WT control littermates. Scale bars: 100 µm in (I) and 20 µm in (H). The illustrations are created with BioRender.com.

Figure 4

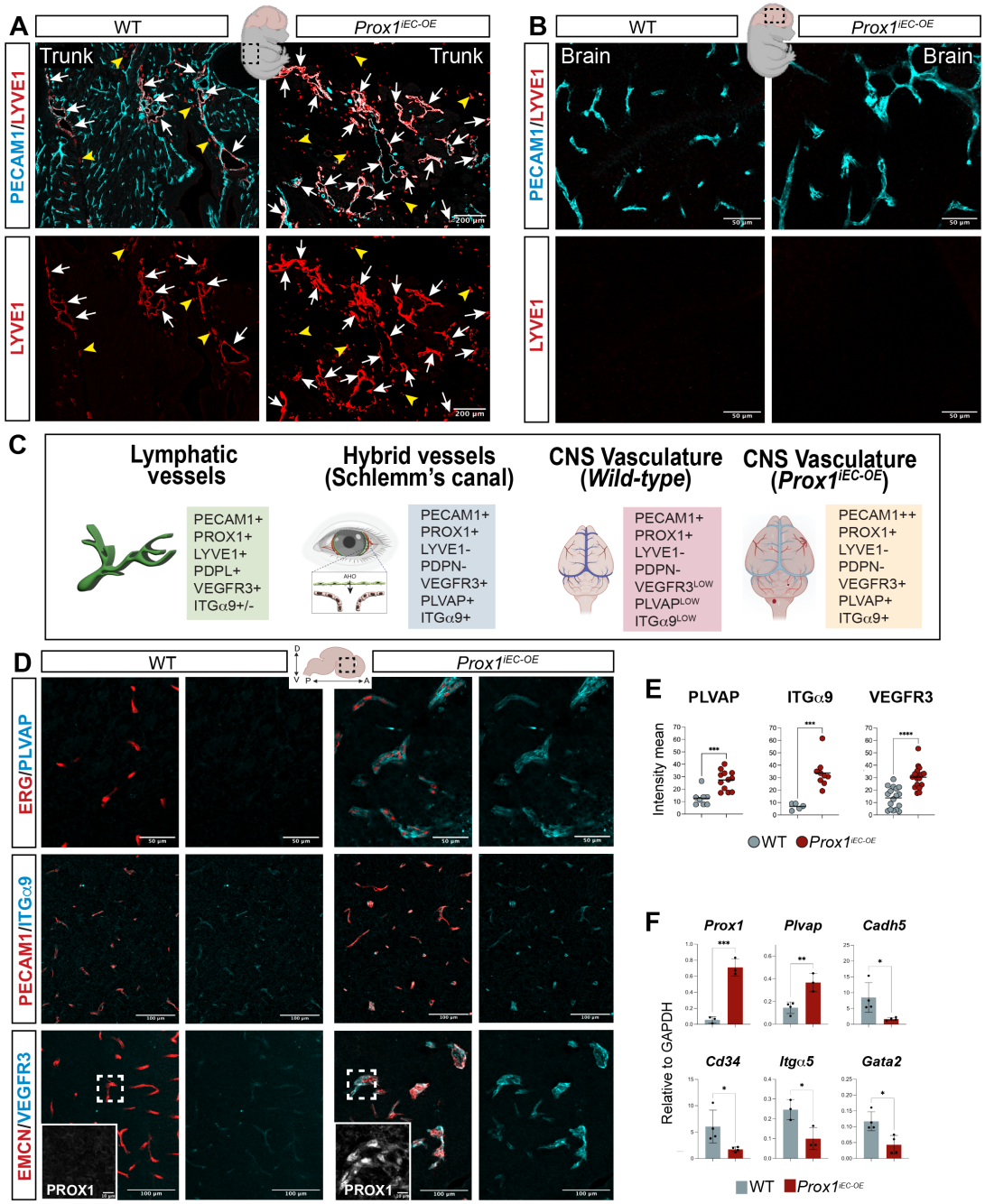

Figure 4. Endothelial *Prox1* expression induces a hybrid blood-lymphatic phenotype in the developing CNS vasculature.
(A-B) Section immunostaining of trunk (A) and brain (B) from E16.5 *Prox1*$^{iEC\text{-}OE}$ mutant and their WT control littermate embryos with PECAM1 (cyan) and LYVE1 (red). Arrows indicate PECAM1+/LVYE1+ lymphatic vessels, while yellow arrowheads indicate PECAM1-/LVYE1+ macrophages. *Prox1*$^{iEC\text{-}OE}$ mutants exhibited enhanced lymphatic differentiation to form PECAM1+/LVYE1+ lymphatic vasculature in the trunk in comparison to their WT control littermates. In contrast, both *Prox1*$^{iEC\text{-}OE}$ mutant and their WT control littermates did not exhibit conventional PECAM1+/LVYE1+ lymphatic vasculature in the brain. Scale bars: 200 µm in (A) and 50 µm in (B). **(C)** Schematic illustrations indicating EC markers expressed in conventional lymphatic vessels, hybrid vessels in the Schlemm's canal, and CNS vessels in WT and *Prox1*$^{iEC\text{-}OE}$ mutants. **(D-E)** Section immunostaining of E16.5 *Prox1*$^{iEC\text{-}OE}$ mutant and their WT control littermate brains with PLVAP (cyan), ITGα9 (cyan) and VEGFR3 (cyan), together with ERG (red), PECAM1 (red), EMCN (red), respectively. The sections labeled with VEGFR3 (cyan) and EMCN (red) are additionally stained with PROX1 (grey in the magnified images). (E) Quantifications of the fluorescence intensity mean for PLVAP, ITGα9 and VEGFR3 in the brain vasculature using Imaris software. Each dot corresponds to random fields of view from at least 3 different WT control and mutant embryos. Data are shown as mean±SEM. Scale bars: 100 µm and 50 µm in (D). **(F)** Relative mRNA expression levels of *Prox1* and *Plvap* together with BEC markers such as *Cadh5, Cd34, Itg*α5, and *Gata2* in FACS-isolated brain ECs from E16.5 *Prox1*$^{iEC\text{-}OE}$ mutant and their WT control littermate brain. Bar graphs show mean normalized expression ±SEM; n=3-4 biological samples obtained from FACS-isolated brain ECs from individual experiments. ** p<0.001, ***p<0.0005, ****p<0.0001, as determined by unpaired t-test. The illustrations are created with BioRender.com.

Figure 5

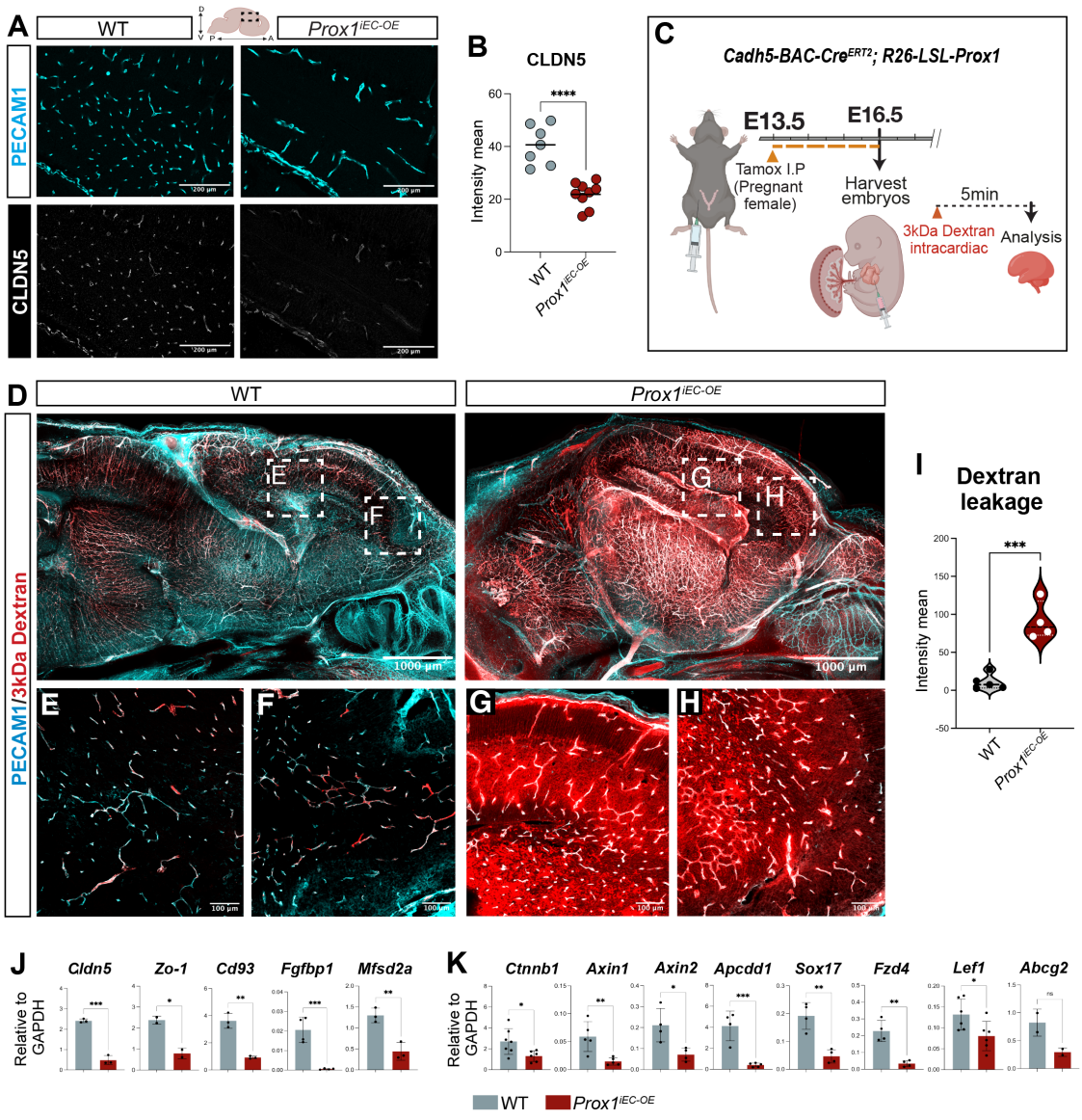

Figure 5. Endothelial *Prox1* expression disrupts the primitive blood-brain barrier formation in the developing CNS vasculature.
(A-B) Section immunostaining of E16.5 *Prox1*$^{iEC\text{-}OE}$ mutant and their WT control littermate brains with PECAM1 (cyan) and CLDN5 (grey). The expression of CLDN5 is downregulated in the brain vasculature of *Prox1*$^{iEC\text{-}OE}$ mutants in comparison to their WT control littermates. (B) Quantifications of the fluorescence intensity mean for CLDN5 in the brain vasculature using Imaris software. Each dot corresponds to random fields of view from at least 3 different WT control and mutant embryos. Data are shown as mean±SEM. ****p<0.0001, as determined by unpaired t-test. Scale bars: 200 µm in (A). **(C)** Diagram depicting EC-specific induction of *Prox1* expression at E13.5 and vascular permeability analysis of embryos at E16.5. **(D-I)** A sagittal view of whole-mount imaging of E16.5 *Prox1*$^{iEC\text{-}OE}$ mutant and their WT control littermate brains with 3kDa Dextran Texas-Red tracer (red) and PECAM1 (cyan). Boxed regions in (D) are magnified in (E and F) as WT control littermates and (G and H) as *Prox1*$^{iEC\text{-}OE}$ mutants. The mutant brains exhibited extensive BBB leakage. (I) Quantification of Dextran Texas-Red tracer extravasation outside of the brain vasculature in WT control (n=5 individual brains, showing the average of 4 different fields of view) and mutant brains (n=4 individual brains, showing the average of 4 different fields of view). ***p<0.0005, as determined by unpaired t-test. Scale bars: 1000 µm in (D) and 100 µm in (E-H). **(J-K)** Relative mRNA expression levels of BBB-related genes such as *Cldn5, Zo-1, Cd93, Fgfbp1*, and *Mfsd2a* in (J), and ß-catenin and its target genes such *Ctnnb1, Axin1, Axin2, Apcdd1, Sox17, Fzd4, Lef1*, and *Abcg2* in (K), in FACS-isolated brain ECs from E16.5 *Prox1*$^{iEC\text{-}OE}$ mutant and their WT control littermate brain. Graphs show mean normalized expression ±SEM; n=3-5 experiments obtained from 4 individual FACS experiments. *p<0.05, ** p<0.001 ***p<0.0005, ****p<0.0001, as determined by unpaired t-test. The illustrations are created with BioRender.com.

Figure 6

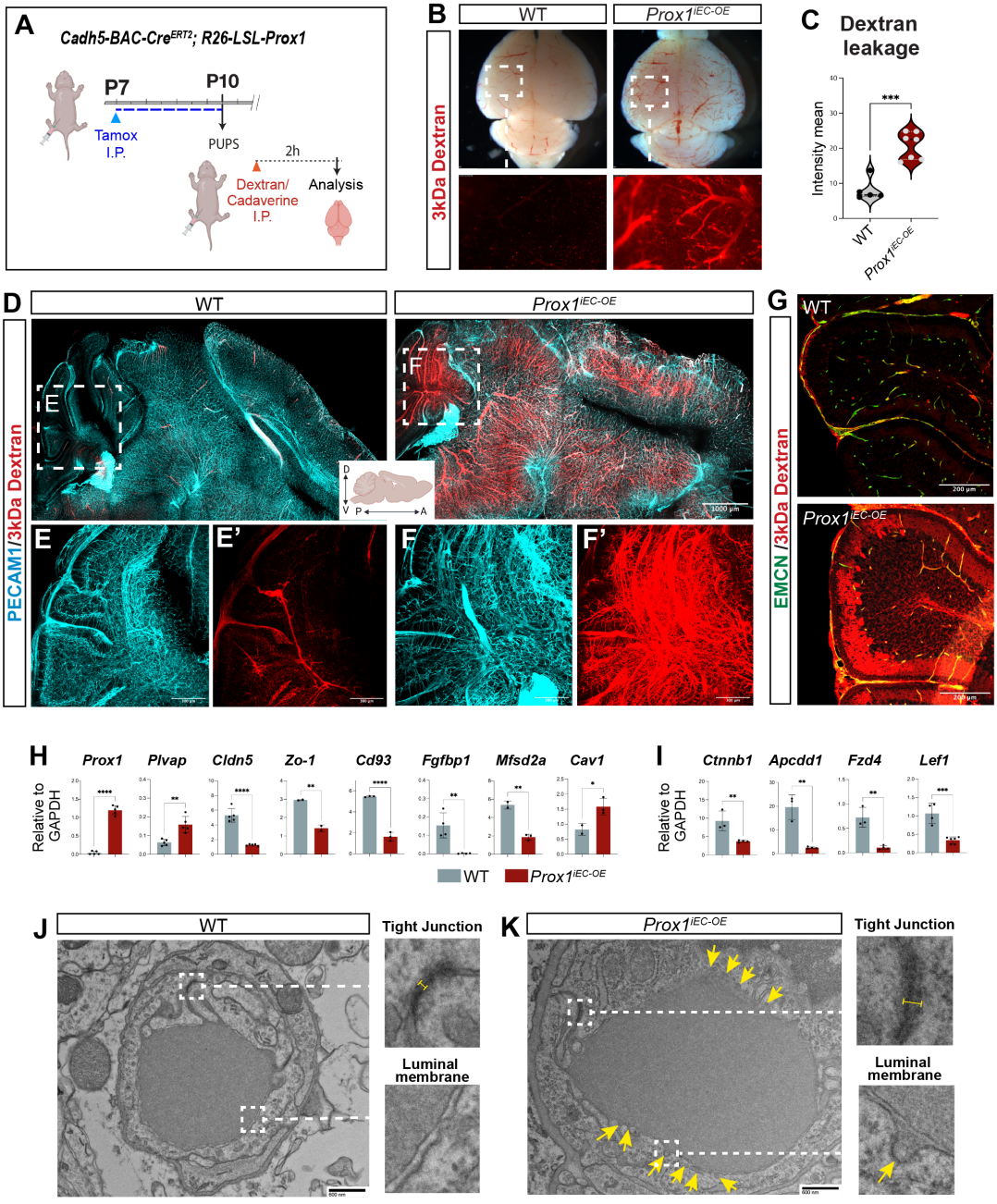

Figure 6. Postnatal induction of *Prox1* disrupts the blood-brain barrier.
(A) Diagram depicting EC-specific induction of *Prox1* expression at P7 and vascular permeability analysis of pups at P10. **(B-C)** Gross appearance of P10 *Prox1*$^{iEC\text{-}OE}$ mutant and their WT control littermate brains with 3kDa Dextran Texas-Red tracer (red). Boxed regions are magnified in the lower panels. (C) Quantification of Dextran Texas-Red tracer outside of the brain vasculature in WT control (n=5 individual brains, showing the average of 4 different fields of view) and mutant brains (n=7 individual brains, showing the average of 4 different fields of view). ***p<0.0005, as determined by unpaired t-test. **(D-F)** A sagittal view of whole-mount imaging of P10 *Prox1*$^{iEC\text{-}OE}$ mutant and their WT control littermate brains with 3kDa Dextran Texas-Red tracer (red) and PECAM1 (cyan). Boxed regions in (D) are magnified in (E-E') as WT control littermates and (F-F') as *Prox1*$^{iEC\text{-}OE}$ mutants. The mutant brains exhibited extensive BBB leakage in the cerebellum. Scale bars: 1000 µm in (D) and 300 µm in (E-F). (G) Section immunostaining of P10 *Prox1*$^{iEC\text{-}OE}$ mutant and their WT control littermate cerebrum with 3kDa Dextran Texas-Red tracer (red) and EMCN (green). Scale bars: 200 µm. **(H-I)** Relative mRNA expression levels of *Prox1* and *Plvap* together with BBB-related genes such as *Cldn5, Zo-1, Cd93, Fgfbp1, Mfsd2a,* and *Cav1* in (H) and ß-catenin and its target genes such *Ctnnb1, Apcdd1, Fzd4*, and *Lef1* in (I), in FACS-isolated brain ECs from P10 *Prox1*$^{iEC\text{-}OE}$ mutant and their WT control littermate brain. Graphs show mean normalized expression ±SEM; n=3-4 biological samples obtained from FACS-isolated brain ECs from individual experiments. ** p<0.001 ***p<0.0005, ****p<0.0001, as determined by unpaired t-test. **(J-K)** Representative transmission electron microscopy (TEM) images of brain capillaries in P10 *Prox1*$^{iEC\text{-}OE}$ mutant and their WT control littermate brain. The boxed regions show tight junctions and luminal membranes are magnified in the right panels. Yellow arrows indicate endothelial vesicles in (K). Scale bars: 600nm in (J and K). The illustrations are created with BioRender.com.

Figure 7

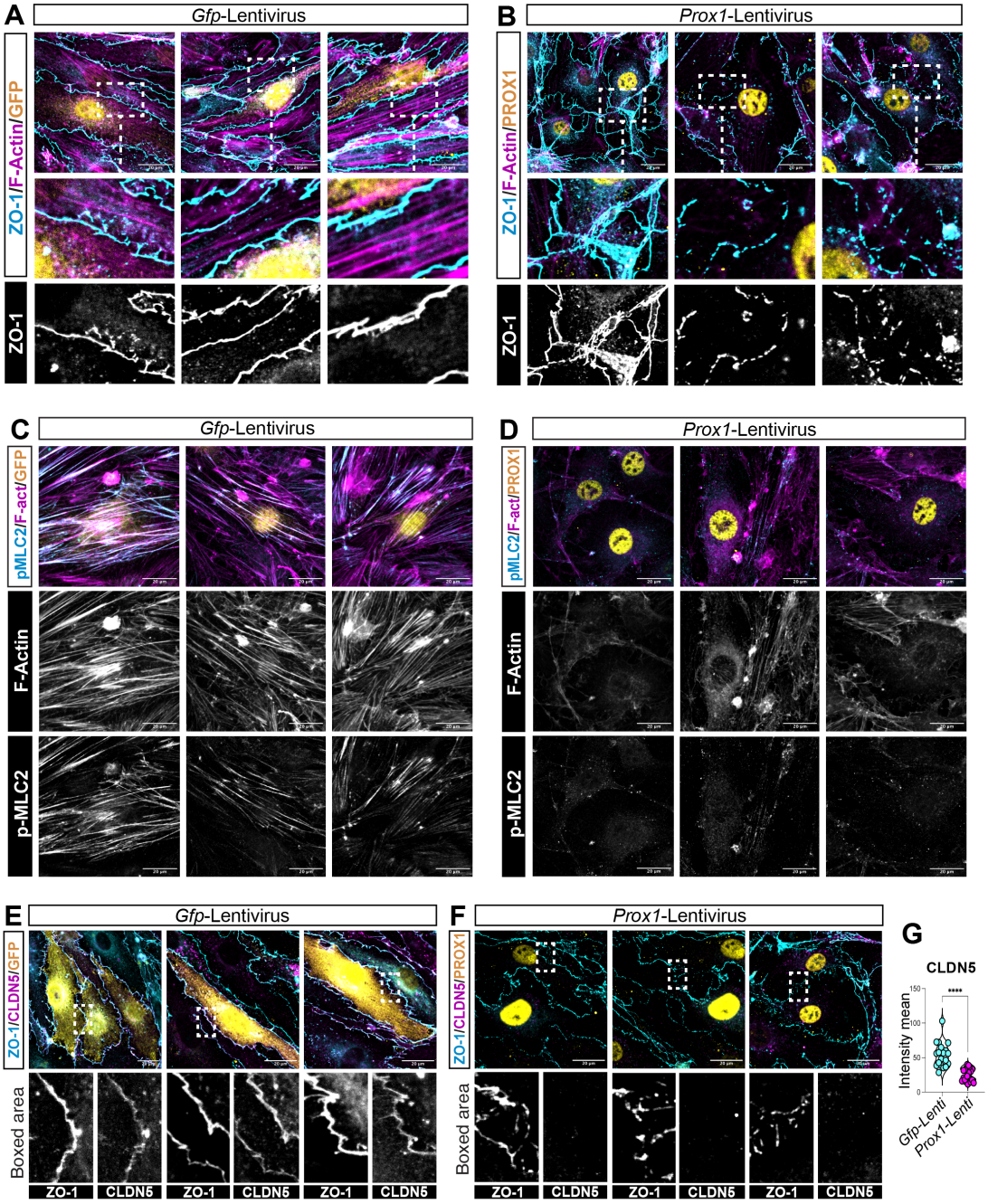

Figure 7. *Prox1* expression induces abnormal tight junctions by repressing *Claudin-5* expression and destabilizing actin filaments in cultured bEnd.3 cells.
(A-B) Three representative images of cultured bEnd.3 mouse brain ECs expressing *Gfp* or *Prox1* labeled with ZO-1 (cyan or grey) and F-Actin (magenta) together with GFP (yellow) or PROX1 (yellow), respectively. Boxed regions are magnified in the lower panels. bEnd.3 cells expressing *Prox1* exhibited discontinuous cell-cell junctions and an enlarged cell shape. **(C-D)** Three representative images of bEnd.3 cells expressing *Gfp* or *Prox1* labeled with p-MLC2 (cyan or grey) and F-Actin (magenta or grey) together with GFP (yellow) or PROX1 (yellow). Both F-Actin and p-MLC2 are downregulated in bEnd.3 cells expressing *Prox1* in comparison to bEnd.3 cells expressing *Gfp*. **(E-G)** Three representative images of bEnd.3 cells expressing *Gfp* or *Prox1* labeled with ZO-1 (cyan or grey) and CLDN5 (magenta or grey) together with GFP (yellow) or PROX1 (yellow). Boxed regions are magnified in the lower panels. bEnd.3 cells expressing Prox1 exhibited a significant reduction of CLDN5 expression. (G) Quantification of the CLDN5 fluorescence intensity in the TJ region. Data are shown as mean ±SEM. n=20 fields of view from 4 independent experiments, ****p<0.0001, as determined by unpaired t-test. Scale bars: 20 µm in (A-F).